STARS

Electronic Theses and Dissertations, 2004-2019

2005

Finite Element Simulation Of Repair Of Delaminated Composite Structures Using Piezoelectric Layers

Kunal Navale
University of Central Florida

STARS Citation

Showcase of Text, Archives, Research & Scholarship

FINITE ELEMENT SIMULATION
OF
REPAIR OF DELAMINATED COMPOSITE STRUCTURES
USING
PIEZOELECTRIC LAYERS

by

KUNAL A. NAVALE
B.E., Maharaja Sayajirao University of Baroda, 1999

A thesis submitted in partial fulfillment of the requirements
for the degree of Master of Science
in the Department of Mechanical Materials & Aerospace Engineering
in the College of Engineering & Computer Science
at the University of Central Florida
Orlando, Florida

Fall Term
2005

ABSTRACT

Damage in composite material fabricated aerospace, aeronautical, mechanical, civil and offshore structures often results from factors such as fatigue, corrosion and accidents. Such damage when left unattended can grow at an alarming rate due to the singularity of the stress and strain in the vicinity of the damage. It can lead to increase in the vibration level, reduction in the load carrying capacity, deterioration in the normal performance of the component and even catastrophic failure. In most conditions, the service life of damaged components is extended with repair instead of immediate replacement. Effective repair of structural damage is therefore an important and practical topic. Repair can extend the service life and can be a cost efficient alternative to immediate replacement of the damaged component.

Most conventional repair methods involve welding, riveting or mounting additional patches on the parent structure without removing the damaged portion. These methods tend to be passive and inflexible, faced with the limitations of adjusting the repair to the changes in external loads. Besides, in certain cases these methods may lead to additional damage to the structure. For example, the in-situ drilling required in some cases can cause damage to items such as hidden or exposed hydraulic lines and electrical cables. Welding or bonding patches can cause significant stress alterations and serious stress corrosion problems, apart from burdening the weight sensitive structures. Above all, effective repair applying conventional analytical methods hinges on calculation of the singularity of stress and strain in the vicinity of the damage, which is be a difficult as only approximate solutions are available. Thus, a need is felt to update the repair

methods with the advancement in fields of materials, sensing and actuating. This can make the repair more effective and efficient than conventional repair methodology.

Current research proposes the use of piezoelectric materials in repair of delaminated composite structures. A detailed mechanics analysis of the delaminated beams, subjected to concentrated static loads and axial compressive loads, is presented. The discontinuity of shear stresses induced at delamination tips due to bending of the beams, under action of concentrated static load and axially compressive load, is studied. This discontinuity of the shear stresses normally leads to the sliding mode of fracture of the beam structures. In order to ensure proper functioning of these beam structures, electromechanical characteristics of piezoelectric materials are employed for their repair. Numerical simulations are conducted to calculate the repair voltage to be applied to the piezoelectric patches to erase the discontinuity of horizontal shear stress at the delamination tips and thus, render the beam repaired. The variation of repair voltage with location and size of the delamination is considered. FE simulations are performed to validate the numerically calculated voltage values. The research presented serves to provide information on the design of piezoelectric materials for the repair of delaminated composite structures.

Dedicated to My Parents!

ACKNOWLEDGMENTS

I would like to extend special thanks to Dr. Quan Wang, my advisor, for his encouragement and valuable advice throughout my research. I would like to express my appreciation to my thesis committee members, Dr. Kuo-Chi "Kurt" Lin and Dr.Gangyi Zhou for all their assistance and cooperation. I would like to thank all my friends for their valuable and unyielding support throughout the completion of my thesis. I would like to thank the MMAE department (Faculty and Staff) for providing me with all the valuable resources, without which this accomplishment would not have been possible. Lastly, I would like to thank my parents and family for their constant love and support, at all times.

TABLE OF CONTENTS

LIST OF FIGURES

LIST OF TABLES

LIST OF ACRONYMS/ABBREVIATIONS

SMA   Smart Material Alloys

PZT   Lead Zirconium Titanate

SS   Simply-supported beam

CL   Cantilever beam

FE   Finite Element

NS   Numerical Simulation

BC   Boundary Condition

CHAPTER 1: INTRODUCTION

In today's world every one wants structures to be lighter, stronger, and more efficient. Both commercial and military aircrafts are being increasingly being made of composite structures, taking the advantage of specific characteristics of composite materials. For example, wings of Grumman X-29 experimental plane, shown in Figure 1, made use of a feature of composites that allows them to bend in one direction but not another. We all use tennis racquets, golf clubs, helmets and much other sporting equipment made of composites. The canoes, boats and fishing gear are being made of composites. Our car fenders are made of composite material to improve shock absorption. Bridges are being repaired with composite patches. The pavement has composite rebar to increase flex and reduce wear and tear. Prosthetics for disabled are being made of composites due to their excellent stiffness but lower weight. In short, today composites materials touch every aspect of our lives.

Figure 1: A Grumman X-29 experimental plane

1.1 Overview of Composite materials

A composite material is basically a combination of two or more materials, each of which retains distinct individual properties. Multiphase metals too are composite materials on a micro scale, but generally the term composite is applied to materials that are created by mechanically bonding two or more different materials together. The resulting material has characteristics that are not characteristic of the components in isolation.

The concept of composite materials is ancient. An example is adding straw to mud for building stronger mud walls. Most commonly, composite materials have a bulk phase, which is continuous, called the matrix; and a dispersed, non-continuous, phase called the reinforcement. Some other examples of basic composites include concrete (cement mixed with sand and aggregate), reinforced concrete (steel rebar in concrete), and fiberglass (glass strands in a resin matrix).

In about the mid 1960's, a new group of composite materials, called advanced engineered composite materials (aka advanced composites), began to emerge. Advanced composites utilize a combination of resins and fibers, customarily carbon/graphite, kevlar, or fiberglass with an epoxy resin. The fibers provide the high stiffness, while the surrounding polymer resin matrix holds the structure together. The fundamental design concept of composites is that the bulk phase accepts the load over a large surface area, and transfers it to the reinforcement material, which can carry a greater load. The significance here lies in that there are numerous matrix materials and as many fiber types, which can be combined in countless ways to produce just the desired

properties. These materials were first developed for use in the aerospace industry because for certain applications they have a higher stiffness to weight or strength-to-weight ratio than metals. This means metal parts can be replaced with lighter weight parts manufactured from advanced composites. For example, the carbon-epoxy composites are two thirds the weight of aluminum, and two and a half times as stiff. Besides, composites are resistant to fatigue damage and harsh environments, and are repairable. Figure 2 shows the Lockheed F-22 plane which employs composites for over a third of its structures.

Figure 2: The Lockheed F-22, using composites for at least a third of its structure

The concept of 'smartness' coupled with the characteristics of composites materials is fast gaining strength these days. Smart composite structures offer the capability to combine the low density, superior mechanical and thermal properties of composite materials along with the inherent capabilities of smart materials to sense and adapt to their environments. Thus, the use of

smart structures (also referred to as intelligent or adaptive structures) offers the potential to significantly improve the performance of aerospace structural components. However, before these materials can be implemented into actual structures, the coupled mechanical, electrical, and thermal behavior of smart materials must be fully characterized. This has led to extensive research since the 1980's to assess both the sensory and active responses of smart materials.

1.2 Overview of Smart Structures

Smart structures are distinguished from conventional structures by the presence of integrated actuator and sensor elements. In a typical smart structure application, the sensors are used to monitor the mechanical response of the structure through changes in the displacements, strains, or accelerations. Once an adverse or undesirable structural response is detected in the sensors, a controller generates the required input to the actuators. The actuators respond to this input and produce a corresponding change in the mechanical response of the structure to a more benign or acceptable state. The capability of smart structures to sense and adapt to their environment leads to a wide range of potential applications including: vibration suppression of aircraft structures; noise control of helicopter rotors; health monitoring of bridges; shape control of large space trusses; aeroelastic control of aircraft lifting components; and seismic control of buildings. Crawley (1993) and Loewy (1997) provide detailed overviews of the current state of smart structures research for aerospace applications

A variety of different materials can be utilized as either sensor or actuator elements in smart structure applications. Depending on the specific material used, the sensor and actuator elements

are controlled through electric, magnetic, thermal, or light energy. Some of the common actuator and sensor materials include: piezoelectric materials, shape memory alloys, fiber optics, electrostrictive materials, magnetostrictive materials, and electro-rheological fluids. Of the different materials available for use in smart structures, only piezoelectric materials have the unique capability to be used effectively as both actuator and sensor elements. Other advantages of piezoelectric materials which help account for their widespread popularity include: simple integration into the structure; a readily obtainable commercial supply of piezopolymers and piezoceramics; and familiarity in using these materials gained from previous applications in transducers.

1.3 Piezoelectric Materials

Historically, piezoelectric materials have been utilized mainly as active structural elements in transducers for application in strain gages, accelerometers, and sonar. Recently, the focus of research has shifted away from the transducer applications toward the development of smart structure applications which combine the active and sensory behavior of piezoelectric materials. The basic characteristics of piezoelectric materials which allow for their use as sensors and actuators are the direct piezoelectric effect, converse piezoelectric effect, and the pyroelectric effect. In the direct piezoelectric effect, the application of a mechanical load on the piezoelectric material induces an electrical response. Through measurement of this electrical response, the mechanical state of deformation in the structure can be determined and monitored, leading to the sensory application. In contrast, the converse piezoelectric effect transforms an electrical input in the piezoelectric material into a corresponding mechanical strain. This leads to the active

applications of piezoelectric materials, in which the state of deformation of the structure can be controlled or altered by applying the appropriate electrical input. The third characteristic behavior is the pyroelectric effect, in which the piezoelectric material responds to changes in temperature by producing an electrical response, which will influence both the direct and converse piezoelectric effects in changing temperature environments.

1.4 Delamination in Composites

Composite materials have been reliably used in many secondary aerospace structures. For example, Graphite/Epoxy composites have been used in primary structures such as wings and tails of the military aircrafts.
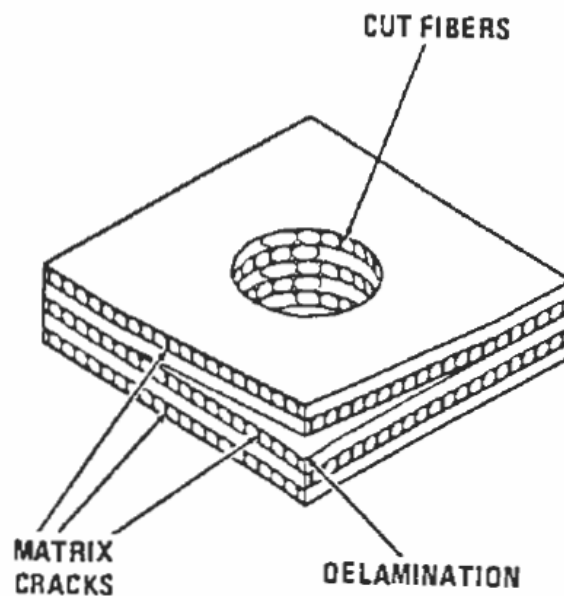
Figure 3: Delamination and other local damage mechanisms in a composite laminate

The primary impediment to full utilization of composites is their inherent tendency to delaminate. Delamination is the most prevalent type of life-limiting failure in composite structures occurring in the form of interlaminar separation or debonds. Technologically, it is also one of the most significant problems in advanced composites. Figure 3 shows a delaminated composite laminate with other kinds of damage mechanisms in composite.

There are various sources of delamination. Delamination may develop during manufacturing with improper consolidation of plies. It may result from impact damage or from three dimensional interlaminar stresses that develop at stress-free edges or discontinuities such as the free surface of a hole. Both interlaminar normal and shear stresses as shown in figure-4 can be detrimental.
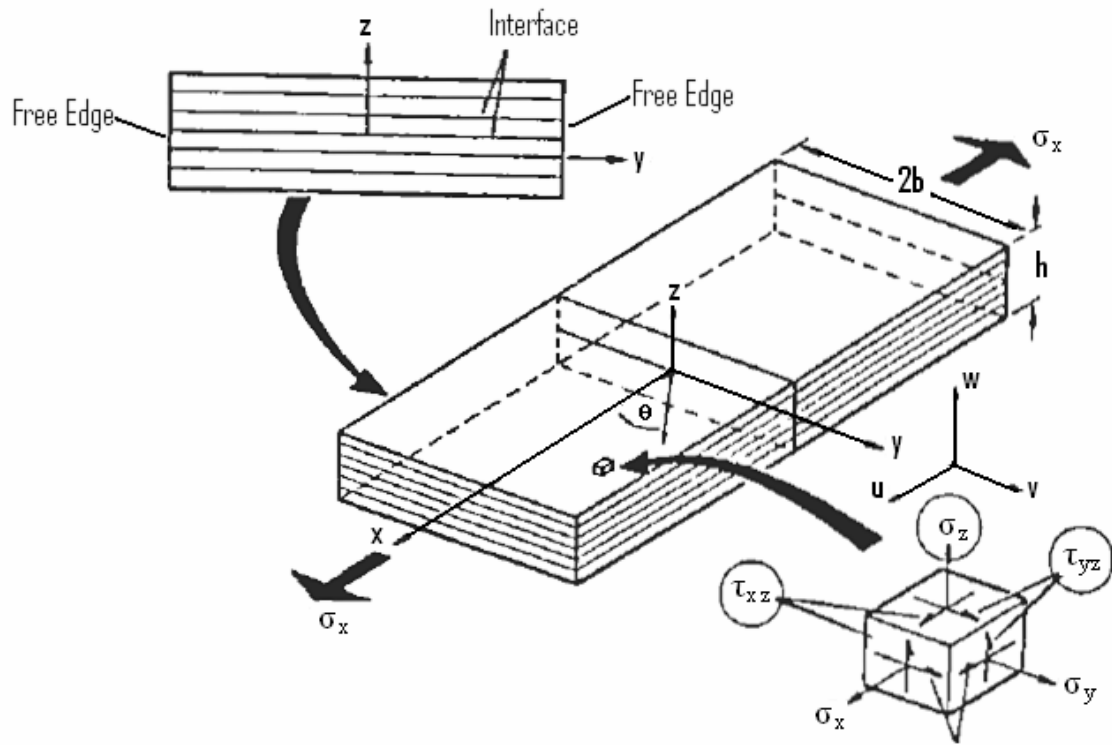
Figure 4: Interlaminar normal and shear stresses in a composite laminate

The interlaminar stresses developing at discontinuities in typical composite structures which may promote delamination are shown in figure 5. Interlaminar stresses can also develop due to compressive loading in laminates. A consequence of compressive loading can be local and global buckling of plies in a laminate. This situation is enhanced due to the propensity of delamination crack growth and the eventual separation of plies.
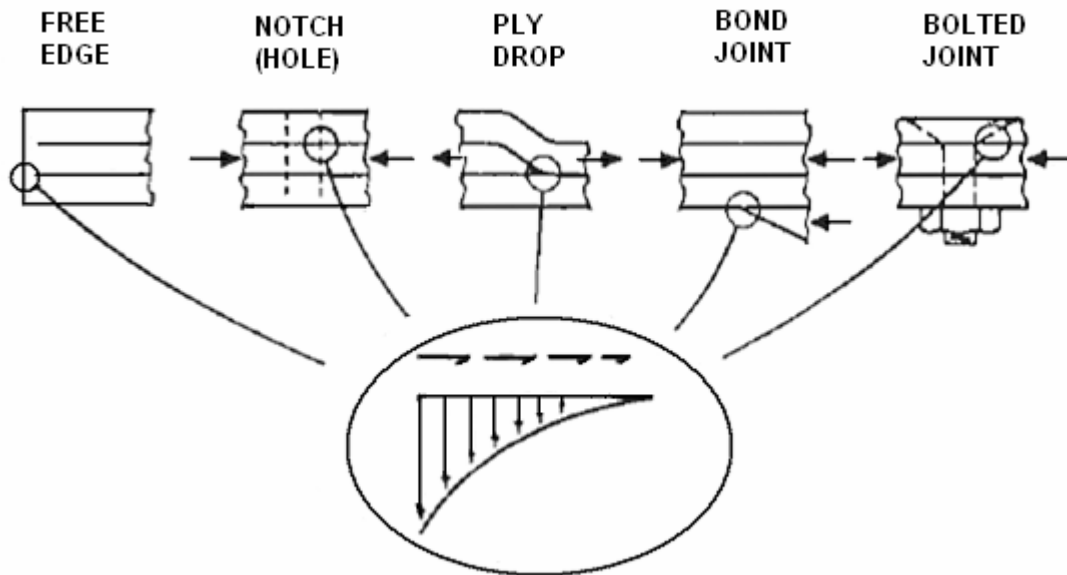
Figure 5: Interlaminar stresses arise from typical discontinuities in composite structures

An area of considerable concern for composites is their response under low velocity impact. Low velocity impact is an important issue since, during servicing, aircraft structures can be damaged due to inadvertent dropping of tool. The damage may not be visible, but internal delamination can be quite extensive resulting in the loss of compression strength and structural integrity. The compressive residual strength of the composite structure may be controlled by the size and location of the delamination.

Fatigue loading is also common in aerospace structures. Delamination initiation and growth due to fatigue is also of concern. An implication is that fatigue propagation life of the structure is short.

Although laboratory characterization of delamination for various modes appears to be quite straightforward, the delamination problem is fairly complex in actual structures. Thus, it is prudent to accurately characterize the onset and growth of delamination in advanced composites. The challenge here rests both on material and structure design fields.

1.5 Research Objectives

With all due considerations given to the design aspects in the field of materials and structures, and with all possible precautions taken, the probability of failure of structure due to delamination arising out of the causes listed earlier still prevails. The current research, thus, assumes delamination in composite structures and proposes a method to check the further growth of delamination, and eventual failure of the structure. It employs piezoelectric materials to repair delaminated composite structures. This method of repair offers many advantages over the conventional repair. For example, piezoelectric materials can repair weight sensitive structures without much added burden because of their light weight. They enable repair adjustments to changes in external loads.

During the current work, a detailed mechanics analysis of the delaminated beams subjected to concentrated static loads and axial compressive loads is presented. The analytical value of repair voltage applied to the piezoelectric layers, surface mounted on delaminated beams with simply supported and cantilever boundary conditions, is proposed. Numerical simulations are performed to study the variation of the repair voltage with the location and size of the delamination. Results from the numerical simulations are validated by the way of FE

simulations using the CAD tool ABAQUS v6.4. The current work provides a comparative analysis of the repair voltage from Numerical and FE simulations and considers the causes for possible deviations. It also considers the future scope of the current study in advanced applications.

CHAPTER 2: LITERATURE REVIEW

The initial use of piezoelectric materials dates back to 1880, when the Curie brothers first discovered the direct piezoelectric effect. Until recently, the use of piezoelectric materials has been limited to a variety of transducer applications. The widespread use of piezoelectric materials as distributed actuators began only in the 1980's, when advances in design and manufacturing technologies made these applications feasible. The experimental work of Bailey and Hubbard (1985) is usually cited as the first application of piezoelectric materials as actuators for vibration control. Using a piezoelectric polymer film as the active element on a cantilevered beam, they were able to demonstrate active damping of the first vibration mode. This new actuator application has led to renewed interest in the development of piezoelectric materials for advanced aerospace structures.

As research into characterizing the active and sensory behavior of piezoelectric materials progressed, a variety of different analytical models were developed. These models can be classified into three broad categories as induced strain models, coupled electromechanical models, and coupled thermo-electromechanical models. The induced strain models use approximate theories to incorporate the piezoelectric effects and are generally limited to predicting only the active response of piezoelectric materials since the electric potential is neglected as a state variable in the formulation. The coupled electromechanical models provide a more consistent representation of both the sensory and active responses of piezoelectric materials by incorporating both the displacements and electric potential as state variables in the formulation. Typically, these models are implemented as finite element codes to provide a more

general analysis tool and a wide variety of different beam, plate, shell, and solid elements have been developed. A natural extension of the coupled electromechanical models is to also incorporate thermal effects. These coupled thermo-electromechanical models include temperature as an additional state variable to account for thermal effects in addition to the piezoelectric effects. A more limited number of finite element codes have been developed with this capability.

2.1 Induced Strain Models

The induced strain models can be separated into two categories: (1) actuator models and (2) actuator and sensor models. The actuator models are concerned only with analyzing the active behavior of piezoelectric materials. They typically approximate the strain generated in the piezoelectric material by an applied electric voltage using statically equivalent forces and moments. The combined actuator and sensor models were developed to include predictions of the sensory response of piezoelectric materials. Although these models introduce the piezoelectric constitutive equations into their formulation, the electric potential is usually not included as a state variable, the conservation of electric flux is not considered in the equations of motion, and the sensory voltages are back calculated using the charge equation.

2.1.1 Actuator Models

Crawley and de Luis (1987) developed an induced strain actuator model for beams. They formulated static and dynamic analytical models based on the governing equations for beams with attached and embedded piezoelectric actuators to model extension and bending.

Experiments were performed on both isotropic and composite cantilevered beams with attached and embedded piezoelectric actuators to validate their models. The study found that segmented actuators are always more effective than continuous actuators since the output of each actuator can be individually controlled. They also showed that embedded actuators in composites degrade the ultimate tensile strength, but have no effect on the elastic modulus. Baz and Poh (1988) investigated methods to optimize the location of piezoelectric actuators on beams to minimize the vibration amplitudes. Numerical studies demonstrated the potential to control vibrations in large flexible structures using a small number of bonded piezoelectric actuators. Im and Atluri (1989) presented a more complete beam model which accounted for transverse and axial deformations in addition to extension and bending. Governing equations were formulated for a beam with bonded piezoelectric actuators for applications in dynamic motion control of large scale flexible space structures.

Tzou and Gadre (1989) formulated an induced strain piezoelectric shell theory. A dynamic model was derived from Love's shell theory for application to multi-layered thin shells with active distributed actuators. A case study was validated with experimental results for the vibration suppression of a cantilevered beam with a piezo-polymer actuator film. Crawley and Anderson (1990) developed a Bernoulli-Euler model to more accurately model actuation induced extension and bending in one-dimensional beams than the model of Crawley and de Luis (1987). The model neglected shear effects and was shown to be best suited for the analysis of thin beams and actuators. Clark et al. (1991) also extended the model of Crawley and de Luis (1987) to study the response of multiple piezoelectric actuators on beam excitations. Based on Euler beam theory, their model was validated with experimental results for the vibration response of a simply

14

supported isotropic beam. The model was found to be best suited for performing initial studies to determine the optimal location of actuators for exciting specific vibration modes.

Crawley and Lazarus (1991) developed induced strain actuation models for plates. Equations of strain actuation were derived for both isotropic and anisotropic plates. Exact solutions were found for simple geometries and boundary conditions, while approximate solutions were used to solve more complex problems. The models were verified with experimental results. Static analysis of a cantilevered composite plate with attached piezo-ceramic actuators were conducted to show the potential for shape control of structures. Dimitriadis et al. (1991) extended the one-dimensional induced strain beam model of Crawley and de Luis (1987) to two-dimensional plates with bonded piezoelectric actuators. Dynamic analyses were performed on simply supported plates to demonstrate the use of actuators to excite selective modes and the influence of actuator geometry on the modal response. Robbins and Reddy (1991) developed a piezoelectric layerwise laminate theory which was implemented into a beam element. Numerical comparisons were conducted using four different displacement theories (two equivalent single layer theories and two layerwise laminate theories) to demonstrate the increased accuracy in displacement and stress predictions obtained from using the layerwise theories.

Mitchell and Reddy (1995b) formulated a power series solution for axisymmetric composite cylinders with either attached or embedded piezoelectric laminas. The solution was verified with finite element analysis. Numerical studies were performed to damp vibrations in truss-type structures using both an embedded cylindrical truss actuator element and an attached actuator patch. Lin et al. (1996) presented an induced actuation plate finite element based on first order

shear deformation theory. Numerical studies were verified with analytical solutions and demonstrated capabilities to control the deflection of composite plates using piezoelectric actuators. Park and Chopra (1996) formulated one-dimensional models to predict the extension, bending, and torsion behavior of beams under piezoelectric actuation. Comparisons with experimental data showed good correlation only for applications in which actuators have low orientation angles (less than 45°) with respect to the beam neutral axis.

Chandrashekhara and Varadarajan (1997) implemented a finite element model for laminated composite beams with integrated piezoelectric actuators derived from a higher order shear deformation theory. Numerical studies investigated the effect of stacking sequence and boundary conditions on the actuator voltages and demonstrated the capability to achieve adaptive shape control of beam structures. Charette et al. (1997) formulated analytical models based on a variation approach to study plates with piezoelectric actuators. The model was specialized for a simply supported plate and used to determine the effects of piezoelectric actuator on the dynamic behavior of the plate. Results of the study were verified with experiments and showed only slight changes in the mode shapes of the plate.

Chattopadhyay and Seeley (1997) implemented a third-order laminate theory into a finite element formulation to investigate piezoelectric actuators. Numerical results were verified with published experimental data. Additional comparisons were conducted to demonstrate the limitations of classical laminate theory in analyzing through-the-thickness stress and strain variations. Librescu et al. (1997) presented a model for composite beams with piezoelectric actuators that included structural tailoring and boundary-moment control. Numerical results

demonstrated the potential to improve the dynamic responses of thin-walled cantilevered structures. Bhattacharya et al. (1998) developed a finite element formulation based on first order shear deformation theory for beams and plates. An eight noded isoparametric piezoelectric element was developed to perform free vibration analysis of laminated composite beams and plates. Numerical studies assessed the impact of stacking sequence, boundary conditions, and applied electric potentials on the free vibration response.

Oguamanam et al. (1998) formulated a piezoelectric composite beam finite element using von Karman nonlinear strain-displacement relations. Numerical studies demonstrated the influence of stress stiffening effects on the natural frequency of slender beams. Tong et al. (1998) developed a two dimensional thin plate finite element to investigate shape control applications. Numerical studies were performed to determine the optimum applied voltage, actuator layout, and actuator number for shape control of composite plates with distributed piezoelectric actuators. Chattopadhyay et al. (1999) implemented a third-order laminate theory into a finite element formulation to investigate the dynamic response of delaminated smart composite plates. Numerical studies were conducted on piezoelectric composite plates with single and multiple delaminations to demonstrate changes in the dynamic response. Hong and Chopra (1999) developed an induced strain plate finite element for composite plates based on classical laminate theory. The model was verified with experimental results and demonstrated the capability to achieve shape control using piezoelectric actuators.

Wang performed extensive studies on the application of piezoelectric layers for repair and enhancement of composite structures. Wang and Quek (2004) studied the application of

piezoelectric patches in the repair of delaminated beams subjected to concentrated static loads. A comprehensive mechanics analysis of the delaminated composite beam was performed to calculate the repair voltage, to be applied to the piezoelectric patches, to eliminate the shear stress singularity at the tips of delamination. The dependence of the voltages on the location and size of the delamination was studied and corresponding numerical simulations were performed. Wang, Zhou and Quek (2005) investigated the repair of delaminated beam subjected to compressive force via piezoelectric layers. The study focused on the elimination of the discontinuity in shear stresses induced at the tips of delamination due to the action of the axial compression. Numerical simulations were performed to arrive at the buckling load of the delaminated beam with different boundary conditions and the repair voltage on the piezoelectric patches. In another study, Wang and Quek (2004) focused on the repair of cracked column under axially compressive load via piezoelectric patch. A model of rotational discontinuity at the crack location was used to develop the analytical buckling solutions and the effect of the crack on the buckling capacity of the damaged column modeled. They employed small piezoelectric patches to induce local moments, and thereby compensate for the decreased buckling capacity of the column structures due to crack. Wang and Wang (2003) considered the buckling enhancement of column strips with piezoelectric layer. They developed the analytical model for obtaining the buckling capacity of the piezoelectric coupled column with general boundary conditions, modeled with different types of spring applied at the ends of the column. The buckling capacity was predicted using Eigen-value solution of the proposed model. The study also considered optimal locations of the piezoelectric layer for higher buckling capacity for the various standard boundary conditions of the column. Wang, Quek and Liew (2002) presented the repair of cracked beam with a piezoelectric patch. The repair voltage to be applied

18

to the piezoelectric patches was developed using simply supported beam as an illustration. The study demonstrated that the required voltage decreases linearly as the distance between the force and the location of the crack is increased. It was also found to vary quadratically with the position of the crack along the length of the beam and decrease hyperbolically as the ratio of the thickness of the piezoelectric patch to that of the beam increased. Wang and Wang (2000) investigated the optimal placement and size of the piezoelectric patches on beams from controllability perspective. They studied the controllability index, which measures the input energy required to achieve a desired structural control by piezoelectric actuators, and observed that an optimal design of the piezoelectric actuator is obtained by maximizing the index. Earlier, Simitses, Sallam and Yin (1985) developed and analyzed a simple one dimensional model for predicting delamination buckling loads. The model was employed to predict the critical loads for delaminated homogeneous plates with both SS and clamped ends. The effects of delamination position, size and thickness on the critical loads were also considered during their study. It was concluded that for certain geometries, the buckling load can serve as a measure of the load carrying capacity of the delaminated configuration.

2.1.2 Actuator and Sensor Models

Lee and Moon (1989) studied the control and sensing of bending and torsional deformations produced by an applied electric field using piezopolymer bimorphs. The experimental results validated the analytical model and demonstrated the use of piezopolymers as actuators. Lee (1990) developed a model that incorporated the piezoelectric constitutive relations. The model was based on classical laminated plate theory and was able to predict both the active and sensory

behavior of piezoelectric materials. Lee et al. (1991) investigated the use of sensor actuator pairs for active damping control. Experimental studies were conducted on the active damping control of the first mode of a cantilevered plate using a sensor and actuator pair to validate the piezoelectric plate theory.

Chandrashekhara and Agarwal (1993) developed a laminated piezoelectric plate element based on a first-order shear deformation theory applicable to both thin and moderately thick laminates. Numerical results were verified with previously published results for a cantilevered plate with attached piezoceramic actuators subjected to a static electric field. Hwang and Park (1993) developed a piezoelectric plate element based on classical laminate theory and Hamilton's principle. The piezoelectric constitutive relations were used to formulate a four noded, two-dimensional quadrilateral plate element for both sensory and active applications. Case studies were performed to investigate the static response of a piezoelectric bimorph beam and the vibration control of a cantilevered plate with attached piezoelectric sensors and actuators. Koconis et al. (1994a, 1994b) developed separate analytical models to investigate the sensory and active behavior of piezoelectric composite beams, plates, and shells. One model is used to predict the change in shape when a specified electric voltage is applied to the actuator, while the second model is used to determine the electric voltages necessary to achieve a desired shape. Both models were formulated using a two dimensional, linear, shallow shell theory which includes transverse shear effects and validated with other numerical, analytical, and experimental results.

20

Sung et al. (1996) derived sensor and actuator equations for a cylindrical piezoelectric composite shell. Based on classical laminate theory, these equations formed the basis of a sensor and actuator design methodology to control flexural and torsional vibrations in cylindrical shells. This methodology was used to design an experimental rig to demonstrate capabilities of the modal sensor and actuator to monitor and control the different vibration modes. Lam et al. (1997) developed a finite element model based on classical laminated plate theory for the active vibration control of composite plates with distributed piezoelectric actuators and sensors. Numerical studies were conducted on a cantilevered composite plate to demonstrate capabilities for static and dynamic analysis. Plettner and Abramovich (1997) implemented a consistent methodology based on Kirchoff-Love thin shell theory to model the static and dynamic response of anisotropic laminated piezoelectric shells. The formulation replaced the induced piezoelectric strain with an equivalent mechanical load. The model was verified with experimental and finite element results for a rectangular isotropic plate.

Peng et al. (1998) implemented a beam finite element using a third order laminate theory for active vibration control of piezoelectric composite beams. Numerical studies were conducted to assess shape control applications and to investigate the effect of sensor and actuator locations on the response of the beam. Liu et al. (1999) formulated a plate finite element based on classical laminated plate theory for modeling the static and dynamic response of composite plates containing piezoelectric actuators and sensors. Numerical studies were conducted to verify the model with results from previously developed models and to study the influence of stacking sequence and sensor/actuator position on the response of composite plates.

2.2 Coupled Electromechanical Models

Attempts to develop a more comprehensive representation of piezoelectric material behavior led to the development of more consistent models that captured the coupled response between the mechanical and electrical behavior. In these coupled models, the charge equation is incorporated into the equations of motion and the electric potential is introduced as an additional degree of freedom in the analysis. These models are generally also implemented as finite element programs to provide a more flexible and general purpose analytical tool.

2.2.1 Analytical Models

Mitchell and Reddy (1995a) formulated a refined hybrid theory for laminated piezoelectric composite plates. The displacement fields are modeled using third order shear deformation theory while electric potentials are represented using a layerwise laminate theory. An analytical solution was developed for simply supported boundary conditions and numerical results demonstrated the limitations of the induced strain methods in modeling thick laminates. Heyliger and Saravanos (1995) developed exact solutions to predict the vibration characteristics of simply supported laminated piezoelectric plates. Numerical studies were conducted to determine the influence of different laminations and aspect ratios on the natural frequencies and mode shapes. Batra and Liang (1997) developed three-dimensional elasticity solutions for the simply supported rectangular laminated plate with embedded piezoelectric layers. Numerical studies examined the steady state vibration of both thin and thick plates containing one actuator layer and one sensor layer.

2.2.2 Finite Element Models

Allik and Hughes (1970) introduced a three-dimensional tetrahedron element in the finite element formulations. Derived at a time when piezoelectric materials were used mainly as crystals in transducer applications, the finite element formulation incorporated the piezoelectric constitutive relations and demonstrated the potential advantages of utilizing the finite element method. Naillon et al. (1983) formulated a finite element model to study the resonance phenomena of single piezoelectric structures typically used in ultrasonic transducers. Numerical studies were performed on the resonance characteristics of two-dimensional parallelepiped bars to assess potential applications in the design of ultrasonic probes. Lerch (1990) formulated two and three dimensional finite elements for performing vibrational analysis of piezoelectric sensors and actuators. The models were verified with experimental data. The natural frequencies and mode shapes of various piezoelectric based laminated composite structures were determined and used to optimize applications as transducers.

Tzou and Tseng (1990) developed a thin piezoelectric solid element. Derived from Hamilton's principle and the piezoelectric constitutive relations, the element is specifically formulated for thin plate and shell structures with distributed piezoelectric sensors and actuators. Numerical studies were performed on the vibration response of a cantilevered plate with both an active and sensory layer of polymeric piezoelectric material. Lammering (1991) developed a piezoelectric shell element. Based on the Reissner-Mindlin shell theory and incorporating the piezoelectric constitutive equations, a shell element was formulated for thin shell structures with attached piezoelectric layers. Case studies were conducted on a cantilevered beam with an attached

23

piezoelectric polymer layer. Ha et al. (1992) formulated a three-dimensional brick element. Using a variational principle and the piezoelectric constitutive relations, they developed an eight-noded solid element. Results from static and dynamic case studies were verified with experimental results for composite plates with attached piezoceramic actuator and sensor patches.

Heyliger et. al. (1994) implemented a layerwise laminate theory into a finite element formulation for plates. Two separate layerwise models were developed which incorporated the coupled equations of piezoelectricity to account for both the active and sensory behavior of laminated plates with piezoelectric layers. Numerical results for a simply supported composite plate with attached polymer piezoelectric layers were verified with exact solutions. Ray et al. (1994) developed a two-dimensional quadrilateral element using a higher order laminated plate theory. An eight-noded quadratic isoparametric quadrilateral element was formulated. Results from the static analysis of a simply supported cross-ply laminated plate bonded with a piezoelectric polymer were verified using previously reported exact solutions. Shieh (1994) developed a multiaxially active and sensory laminated piezoelectric beam element. Based on adjusted elementary beam assumptions to account for warping effects, the element can simultaneously model axial extension, biaxial bending, and torsional twisting of the beam. Numerical studies were performed on a space antenna frame to demonstrate capabilities for three-dimensional multiaxial vibration control.

Saravanos and Heyliger (1995) developed a layerwise finite element formulation for beams. Two separate theories were used to perform static and free vibration analysis of composite beams.

Numerical results were verified with previously published analytical studies and demonstrated the increased accuracy of stress-strain predictions with the layerwise theory. Shen (1995) developed a finite element formulation for beams containing piezoelectric actuators and sensors. Based on Timoshenko beam theory, the methodology captured the coupling between the longitudinal and bending motions. The theory was validated with previously published analytical results for a piezoelectric polymer bimorph beam and experimental results for a cantilevered beam with attached piezoelectric sensors and actuators. Suleman and Venkayya (1995) formulated a plate element for analyzing composite plates with layered piezoelectric actuators and sensors. Based on classical laminate theory, a four-noded bilinear Mindlin plate element was developed. Previously published experimental and analytical results for a cantilevered piezoelectric bimorph beam and a cantilevered composite plate with distributed piezoelectric actuators were used to validate the formulation.

Donthireddy and Chandrashekhara (1996) also formulated a layerwise theory for beams. Results from the static response of a cantilevered composite beam with attached piezoelectric actuators were validated with previous analytical results. Additional parametric studies were conducted to study the influence of boundary conditions and ply orientation on the shape control of beams. Heyliger et al. (1996) implemented a layerwise laminate theory into a finite element formulation for shells. Results were verified with exact solutions for the static and free vibration response of a simply supported plate. Additional studies were performed on the active and sensory response of a cylindrical shell. Kim et al. (1996) developed a transition element to connect three dimensional solid elements to flat shell elements. The reported approach used solid elements to provide detailed models of the piezoelectric material, while flat shell elements were used to

25

provide a more flexible model for the substrate structure, and transition elements were used to connect the two regions. The model was verified experimentally for a cantilevered plate.

Samanta et al. (1996) extended the eight-noded quadrilateral element developed by Ray et al.(1994) for dynamic analysis. Based on a higher order shear deformable displacement theory, the model was developed for active vibration control of laminated plates with integrated piezoelectric layers. Numerical results were performed on a simply supported cross-ply plate with attached piezopolymer layers to demonstrate the potential to achieve significant reductions in vibration amplitude. Kim et al. (1997) provided additional details of the theoretical development of the transition element reported by Kim et al. (1996). Numerical studies were conducted to demonstrate convergence characteristics and to show the increased computational efficiency of this approach Saravanos (1997) presented a shell element for curvilinear piezoelectric laminates which combined a first order shear deformation theory for the displacements along with a layerwise theory for the electric potential. The quadratic element was intended for static and dynamic analysis of thin to moderately thick shell structures. Numerical studies quantified the effects of curvature on the active and sensory response of piezoelectric shells.

2.3 Coupled Thermoelectromechanical Models

All of the previously described models neglect the implication of thermal effects on both the active and sensory response of piezoelectric structures. Although Mindlin (1974) derived the two dimensional thermo-piezoelectric equations for plates over twenty years ago, only limited

research has been performed into this area. The development of models for thermo-piezoelectric materials can be separated into two categories: (1) analytical models and (2) finite element models. The analytic models extend existing piezoelectric laminate theories to account for thermal effects and obtain solutions for specific problems. The finite element models provide a more general purpose tool to efficiently analyze complex problems.

2.3.1 Analytical Models

Tauchert (1992) developed a thermo-piezoelectric laminate plate theory. His theory extended classical laminate theory to account for thin laminated plates with thermo-piezoelectric layers. Specific solutions were developed for both free and simply supported composite plates with attached piezoelectric polymer layers. Numerical results demonstrated the capability to reduce thermal deformations through application of active electric voltages. Tzou and Howard (1994) formulated a thermo-piezoelectric thin shell theory for applications to active structures. The generic shell theory was derived using Kirchoff-Love shell theory and Hamilton's principle. Using a simplification procedure based on the Lame parameters and radii of curvatures, specific solutions were obtained for a cylindrical piezoelectric ring, a piezoelectric ring, and a piezoelectric beam. Tang and Xu (1995) developed dynamic solutions for a simply supported anisotropic piezo-thermoelastic composite plate. The coupling between the elastic field and the electric and thermal fields were neglected to simplify the analysis. Numerical results demonstrated a significant reduction in deflection of a plate by the addition of a piezoelectric layer with a harmonic electric field.

Tzou and Bao (1995) extended the thermo-piezoelectric thin shell theory developed by Tzou and Howard (1994) for applications to anisotropic shell laminates with distributed sensors and actuators. The governing equations were simplified and applied to a thin piezo-thermoelastic laminated shell made of a piezoelectric polymer. Applications demonstrated the coupling between the elastic, electric, and thermal fields and the importance of all three fields on the overall behavior of the shell. Stam and Carmen (1996) presented axisymmetric thermo-electromechanical solutions for concentric piezoelectric cylinders. The analytical approach was used to model the quasi-static response of a linear piezoelectric motor. Results of the study demonstrated the capability to extrapolate the nonlinear dependence of the piezoelectric coefficients with electric fields to lower temperatures using the constitutive equations. Friswell et al. (1997) developed a linear model to investigate active damping of thermally induced vibrations. Numerical studies were conducted on a simply supported aluminum beam with a piezoelectric sensor/actuator pair to demonstrate the influence of pyro-electric effects on vibration control.

2.3.2 Finite Element Models

Rao and Sunar (1993) developed a finite element formulation with applications for integrated sensing and control of thermopiezoelectric materials. Numerical studies were performed on a piezoelectric bimorph beam and an isotropic beam with attached piezoelectric polymer layers. The results demonstrated the significance of thermal effects on the performance of distributed control systems. Jonnalagadda et al. (1994) implemented a nine-noded Lagrangian plate element using a first-order shear deformation theory. Numerical studies were performed on a simply

supported composite plate with an attached piezoelectric active layer and demonstrated the importance of a higher order laminate theory to accurate predict shear deformations in thick laminates. Tzou and Ye (1994) extended the previously developed solid element of Tzou and Tseng (1990) to account for thermal effects. The resulting three-dimensional thin hexahedron element represented the displacements, electric potential, and temperature as state variables. Numerical studies were performed on a cantilevered isotropic beam with attached piezoelectric layers to demonstrate the influence of thermal effects on sensing and control.

Chandrashekhara and Tenneti (1995) developed a nine-noded finite element for active thermal control of composite plates with piezoelectric actuators and sensors. The approach incorporated an induced strain approach to approximate the piezoelectric and thermal strains. Numerical studies demonstrated the capability to suppress thermally induced deformations through the application of electrical voltages in piezoelectric patches. Shen and Weng (1995) implemented a three-dimensional brick finite element to investigate composite plates with piezoelectric layers. Numerical studies demonstrated the significant coupling between the strain and electric fields and the capability to achieve thermal shape control of a simply supported piezoelectric composite plate. Sunar and Rao (1997) formulated finite element equations for the design of thermo-piezoelectric sensors and actuators. Numerical studies were conducted on cantilevered beams with piezoelectric actuators to show the significance of temperature effects on distributed control.

2.4 Summary of current work

The objective of current work is to propose a methodology for the repair of delaminated beams using piezoelectric layers. In order to focus on the principle behind the proposed method, cases of delaminated beam subjected to a concentrated static load and axial compression load are considered. The effect of fracture (in terms of generalized stresses and strains) of the beam due to the existence of the delamination is analyzed first. Numerical simulations are performed to compute the repair voltage applied on the piezoelectric patches surface mounted on the beams. For simplicity purposes, only simply supported and cantilever beams are discussed in the research to illustrate the design of the piezoelectric materials in repair of delaminated structures. Parametric studies on the effect of the location and the size of the delamination on the repair design are performed. Results from the numerical simulations are validated by the way of FE simulations performed using the CAD tool ABACUS v6.4, and due consideration for the deviations between theoretical and simulation results provided. The studies in the current work provide a sound foundation for the application of piezoelectric materials in the repair of delaminated structures.

CHAPTER 3: MECHANICS OF MODEL

This chapter discusses the effect of delamination in composite beam structures subjected to axially compressive loads and concentrated static loads. The cases of SS and CL boundary conditions are considered for analytical formulation and the repair voltage applied on the piezoelectric patches, to eliminate the effect of delamination, is proposed. The discussion is solely based on is on the work done by Wang and Quek (2004) and Wang, Zhou and Quek (2005).

3.1 Current Formulation Assumptions

The current formulation assumes a simple linear elastic model for composites, without considering some other factors, like the post-buckling motion and crack propagation due to perturbations in the loading, in the analysis. Isotropic material properties are assumed for the composite structures and piezoelectric layers and the bonding between the two is assumed to be perfect. That is, the bonding layer has an infinite stiffness.

3.2 Effect of delamination on composite beams

A detailed mechanics analysis is provided for the effect of delamination in composite beam structures. The analysis is valid for both, beams subjected to concentrated static loads and beams subjected to axially compressive loads. Beams with SS and CL boundary conditions are considered for the purpose of analysis. Figures 6 and 7 and show a delaminated beam subjected axially compressive loads and concentrated static loads respectively.

The delamination part is studied via Euler-Bernoulli beam theory by considering two layers of the beam elements connected at the two ends. The interface of the two layers is considered as a connection of two free surfaces. Only bending motion is considered for stability analysis, under action of concentrated static loads or axially compressive loads, as the lateral and axial motions in a beam structure are decoupled. Since the mid-planes of the two layers are off the mid-plane of the delaminated beam, axial elongation and compression on the two layers is induced due to bending of the beam. It is assumed that an incremental tensile force Δp_1 and compressive force Δp_2 is induced on the top and bottom layers of the delamination, during the bending of the beam.

The material and geometric parameters of the delaminated beam considered for analysis are denoted as

E - Young's modulus of the host beam

H - Thickness of the beam

t - Distance of the delamination from the top of the host beam

a - Length of the delamination

L_1 - Distance from left tip of delamination to the left end of the host beam

L_2 - Distance from right tip of delamination to the right end of the host

beam
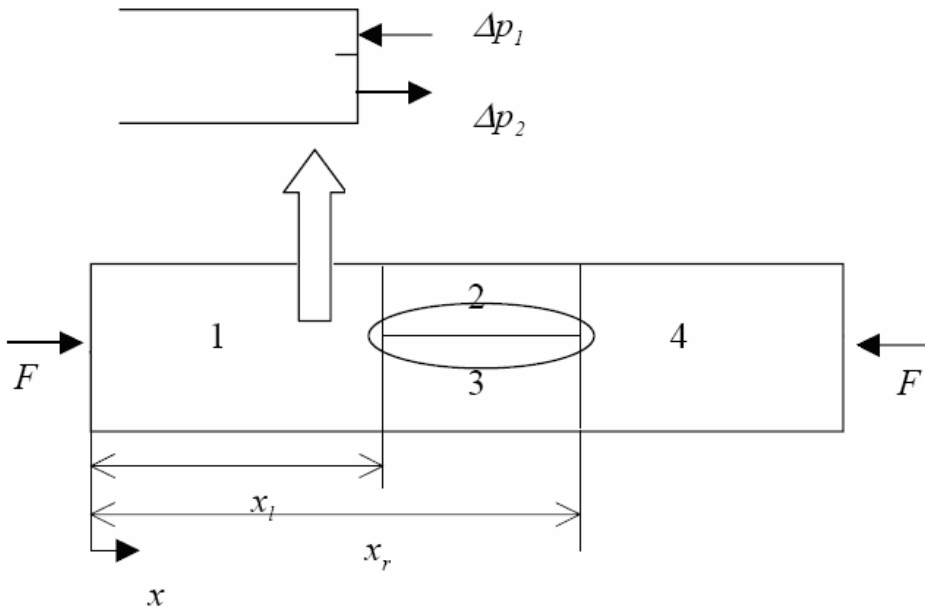
Figure 6: Fracture mechanism at delamination tip for beam subjected to axially compressive load
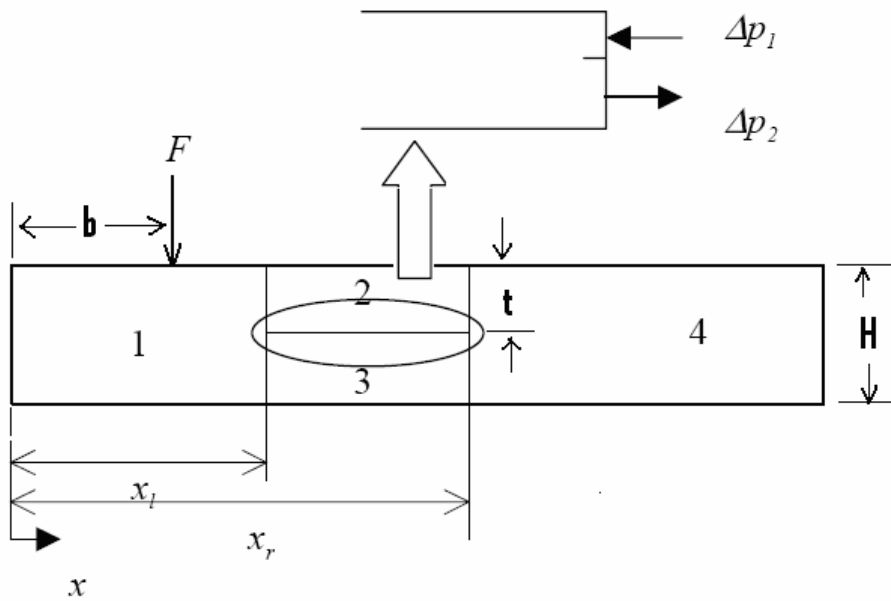
Figure 7: Fracture mechanism at delamination tip for beam subjected to concentrated static load

As shown in the figures 6 and 7, the subscripts 1,2,3,4 are used for entities associated with various sections of the beam as follows:

1 – section from left end of beam to the left of delamination

2 – section above delamination, extending for the entire span of delamination

3 – section below delamination, extending for the entire span of delamination

4 – section from right end of delamination to right end of the beam

The continuity of deflection at the left tip of the delamination based on Euler-Bernoulli beam theory yields:

$$u_{2L} - \frac{1}{2} \left. w_1' \right|_{x=x_l} (H-t) = u_{1L} \tag{1}$$

$$u_{3L} - \left(-\frac{t}{2} \left. w_1' \right|_{x=x_l} \right) = u_{1L} \tag{2}$$

where,

x_l – Coordinate of the left tip of the delamination

w_1 – Flexural deflection/mode shape of the beam element on the left side of

the delamination; the prime indicates the derivative with respect to x

u_{2L} – Horizontal deflection/mode shape of mid-plane of the upper layer of the

delamination at the left tip

u_{3L} – Horizontal deflection/mode shape of mid-plane of the lower layer of the

delamination at the left tip

u_{1L} – Horizontal deflection/mode shape of the mid-plane of the delaminated beam

at the left tip of the beam

Similarly at the right tip of the delamination, we have,

$$u_{2R} - \frac{1}{2} w_4' \Big|_{x=x_r} (H - t) = u_{4R} \tag{3}$$

$$u_{3R} - \left(-\frac{t}{2} w_4' \Big|_{x=x_r} \right) = u_{4R} \tag{4}$$

where,

x_r – Coordinate of the right tip of the delamination

w_4 – Flexural deflection/mode shape of the beam section at the right side of the

delamination; the prime indicates the derivative with respect to x

u_{2R} – Horizontal deflection/mode shape of the mid-plane of upper layer of

delamination at the right tip

u_{3R} – Horizontal deflection/mode shape of the mid-plane of the lower layer of the

delamination at the right tip

u_{4R} – Horizontal deflection/mode shape of the mid-plane of the delaminated beam

at the right tip of the beam

According to the elastic theory, the elongation and the compression of the mid-planes of the upper and lower layers is respectively expressed as:

$$u_{2R} - u_{2L} = \frac{\Delta p_1 a}{EtT} \tag{5}$$

$$u_{3R} - u_{3L} = -\frac{\Delta p_2 a}{E(H-t)T}$$ (6)

where,

      T is the width of the beam.

The characteristic of the non-deformable mid-plane of the delaminated beam implies

$$u_{4R} - u_{1L} = 0$$ (7)

Comparison of the equations (1), (2), (3), (4), (5), (6) and (7) leads to

$$\frac{\Delta p_1 a}{EtT} + \frac{\Delta p_2 a}{E(H-t)T} = -\frac{H}{2}\left(w_1' \Big|_{x=x_l} - w_4' \Big|_{x=x_r} \right)$$ (8)

$$\Delta p_1 = \Delta p_2$$ (9)

From equations (8) and (9) we have,

$$\Delta p_1 = \Delta p_2 = -\frac{ETH\beta}{2a}\left(w_1' \Big|_{x=x_l} - w_4' \Big|_{x=x_r} \right)$$ (9a)

where,

$$\beta = \left(\frac{1}{t} + \frac{1}{(H-t)} \right)^{-1}$$ (10)

Thus, it is seen that the tensile and compressive forces are induced at the upper and lower layers of the delamination due to bending of the beam under the action of concentrated static load or axially compressive load. These induced tensile and compressive forces lead to the discontinuity of the shear forces at the tips of the delamination, which further results into sliding mode of fracture of the beam at the delamination tips. To avoid the sliding mode of fracture, and thus

render the beam repaired, it is required to induce counter forces to balance the shear forces at the tips of delamination.

3.3 Buckling analysis of delaminated beams

This section provides a simple mechanics model for the buckling solution of delaminated beams. SS and CL beams subjected to axially compressive load are considered for illustration purpose. Only the lower order Eigen-value problem is considered to arrive at the solution by the way of sectional analysis as shown in the figure 6. Earlier, Simitses, Sallam, and Yin (1985) performed the buckling analysis of delaminated beam structures. During their study too, a sectional method was adopted and perturbation technique was used in deriving the buckling results. The effect of delamination was not explicitly addressed in their study. Besides, a complicated model, involving more efforts, was proposed to arrive at the buckling solution.

Referring to figure 6, the governing equation for section 1 of the delaminated beam is given by:

$$EI \frac{d^4 w_1(x_1)}{dx_1^4} + F \frac{d^2 w_1(x_1)}{dx_1^2} = 0 \qquad\qquad 0 \leq x_1 \leq L_1 \tag{11}$$

where,

I is the area moment of inertia expressed as:

$$I = \frac{H^3 T}{12} \tag{12}$$

and A is the area of the cross-section of the beam expressed as:

$$A = HT \tag{13}$$

37
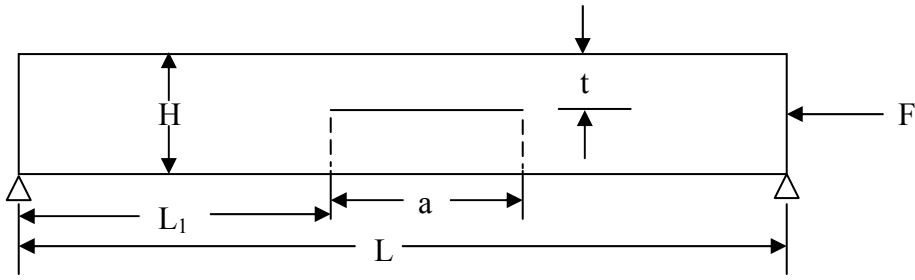
Figure 8: Delaminated SS beam subjected to compressive load
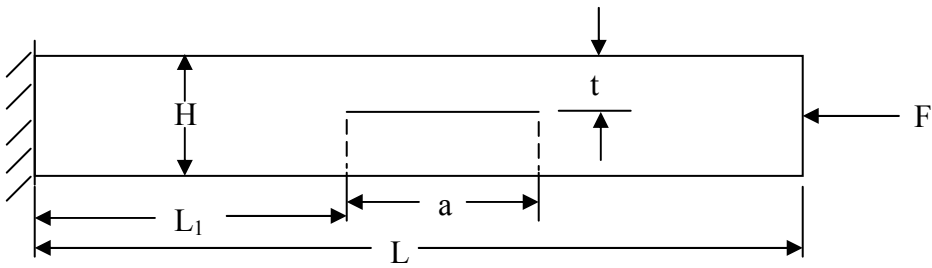
Figure 9: Delaminated CL beam subjected to compressive load

For SS and CL beams shown in figures 8 and 9, the two types of boundary conditions on the left end are pinned and fixed respectively. These are mathematically expressed as follows:

For Pinned end:

$$w_{11}(0) = 0 \tag{14}$$

and

$$\left. \frac{d^2 w_{11}(x_1)}{dx_1^2} \right|_{x_1=0} = 0 \tag{15}$$

For Fixed end:

$$w_{12}(0) = 0 \tag{16}$$

and

$$\left. \frac{d \; w_{12}(x_1)}{dx_1} \right|_{x_1=0} = 0 \tag{17}$$

The general solution for $w_1(x_1)$ satisfying the governing equation (11) and boundary conditions at the left end is expressed as:

For Pinned end:

$$w_{11}(x_1) = A_{11}\sin \lambda \, x_1 + A_{21} x_1 \tag{18}$$

For Fixed end:

$$w_{12}(x_1) = A_{12}(\cos \lambda \, x_1 - 1) + A_{22}(\sin \lambda \, x_1 - \lambda \, x_1) \tag{19}$$

where,

$$\lambda = \sqrt{\frac{F}{EI}} \tag{20}$$

and

A_{1i} and A_{2i} ($i=1,2$) are coefficients.

Similarly, the expressions for the mode shape function $w_4(x_4)$ on section 4, where ($0 < x_4 < L_2$), are provided by considering the boundary conditions on the right end of the beams. The boundary conditions at the right ends for the beams in figures 8 and 9 are pinned and free respectively. These are mathematically expressed as follows:

39

For Pinned end:

$$w_{41}(L_2) = 0 \tag{21}$$

and

$$\frac{d^2 w_{41}(x_4)}{dx_4^2}\bigg|_{x_4=L_2} = 0 \tag{22}$$

For Free end:

$$\frac{d^2 w_{43}(x_4)}{dx_4^2}\bigg|_{x_4=L_2} = 0 \tag{23}$$

and

$$\frac{d^3 w_{43}(x_4)}{dx_4^3}\bigg|_{x_4=L_2} + \lambda^2 \frac{d\ w_{43}(x_4)}{dx_4}\bigg|_{x_4=L_2} = 0 \tag{24}$$

The corresponding general solutions for $w_{4j}(x_4)$, $(j=1,3)$ satisfying the same governing equation

(11), and two boundary conditions shown above are given by:

For Pinned end:

$$w_{41}(x_4) = D_{11}(-\sin \lambda L_2 \cos \lambda x_4 + \sin \lambda x_4 \cos \lambda L_2) + D_{21}\left(1 - \frac{x_4}{L_2}\right) \tag{25}$$

For Free end:

$$w_{43}(x_4) = D_{13}(\sin \lambda L_2 \cos \lambda x_4 - \sin \lambda x_4 \cos \lambda L_2) + D_{21} \tag{26}$$

where,

D_{1j}, D_{2j} and D_{3j} $(j=1,3)$ are coefficients.

40

The delamination is viewed as the free surface between the upper and lower layers since shear motions for the two layers are free at the interface (Simitses, Sallam, and Yin, 1985). The governing equations for the delamination part, that is, for the upper and lower layers are expressed as:

$$E I_1 \frac{d^4 w_2(x_2)}{d x_2^4} + F_1 \frac{d^2 w_2(x_2)}{d x_2^2} = 0 \quad \text{for } 0 \le x_2 \le a \tag{27}$$

$$E I_2 \frac{d^4 w_3(x_2)}{d x_2^4} + F_2 \frac{d^2 w_3(x_2)}{d x_2^2} = 0 \quad \text{for } 0 \le x_2 \le a \tag{28}$$

where,

$$
\begin{aligned}
I_1 &= I \bar{t}^3 \\
I_2 &= I (1-\bar{t})^3 \\
F_1 &= F \bar{t} \\
F_2 &= F(1-\bar{t}) \\
A_1 &= A \bar{t} \\
A_2 &= A(1-\bar{t}) \\
\bar{t} &= \frac{t}{H}
\end{aligned}
\tag{29}
$$

The general solution for the mode shapes, $w_2(x_2)$ and $w_3(x_2)$, is:

$$w_2(x_2) = B_1 \cos \lambda_1 x_2 + B_2 \sin \lambda_1 x_2 + B_3 x_2 + B_4 \tag{30}$$

$$w_3(x_2) = C_1 \cos \lambda_1 x_2 + C_2 \sin \lambda_1 x_2 + C_3 x_2 + C_4 \tag{31}$$

where,

$$\lambda_1 = \sqrt{\frac{F_1}{E I_1}} = \frac{\lambda}{\bar{t}} \tag{32}$$

$$\lambda_2 = \sqrt{\frac{F_2}{EI_2}} = \frac{\lambda}{(1-\bar{t})} \tag{33}$$

and

B_k, C_k ($k=1,2,3,4$) are the coefficients

The continuity equations for the deflection and rotation at the interface of section 1 and section 2 are expressed as:

$$w_1(L_1) = w_2(0) \tag{34}$$

$$\left. \frac{d\ w_1(x_1)}{dx_1} \right|_{x_1=L_1} = \left. \frac{d\ w_2(x_2)}{dx_2} \right|_{x_2=0} \tag{35}$$

Similarly, at the interface of section 1 and section 3 the continuity equations for the deflection and rotation are expressed as:

$$w_1(L_1) = w_3(0) \tag{36}$$

$$\left. \frac{d\ w_1(x_1)}{dx_1} \right|_{x_1=L_1} = \left. \frac{d\ w_3(x_2)}{dx_2} \right|_{x_2=0} \tag{37}$$

The tensile and compressive forces are induced at the upper and lower layers of the delamination induce additional moment given by:

$$\Delta M = \Delta p_1 \left(\frac{H-t}{2} \right) + \Delta p_2 \frac{t}{2} = \frac{\Delta p_1 H}{2} \tag{38}$$

Thus, the discontinuity of the moment and the continuity of the shear force at both the interface of section 1 and section 2 and the interface of section 1 and section 3 are expressed as follows by considering the expressions of Δp_1 in equation (9a):

$$EI \frac{d^2 w_1(x_1)}{dx_1^2}\bigg|_{x_1=L_1} = EI_1 \frac{d^2 w_2(x_2)}{dx_2^2}\bigg|_{x_2=0} + EI_2 \frac{d^2 w_3(x_2)}{dx_2^2}\bigg|_{x_2=0} + \frac{\Delta p_1 H}{2} \tag{39}$$

which can be written as:

$$\frac{d^2 w_1(x_1)}{dx_1^2}\bigg|_{x_1=L_1} = \bar{t}^3 \frac{d^2 w_2(x_2)}{dx_2^2}\bigg|_{x_2=0}$$

$$+ (1-\bar{t})^3 \frac{d^2 w_3(x_2)}{dx_2^2}\bigg|_{x_2=0} - \frac{\beta(w_1'(L_1) - w_4'(0))}{3a} \tag{40}$$

And,

$$EI \frac{d^3 w_1(x_1)}{dx_1^3}\bigg|_{x_1=L_1} = EI_1 \frac{d^3 w_2(x_2)}{dx_2^3}\bigg|_{x_2=0} + EI_2 \frac{d^3 w_3(x_2)}{dx_2^3}\bigg|_{x_2=0} \tag{41}$$

which can be written as:

$$\frac{d^3 w_1(x_1)}{dx_1^3}\bigg|_{x_1=L_1} = \bar{t}^3 \frac{d^3 w_2(x_2)}{dx_2^3}\bigg|_{x_2=0} + (1-\bar{t})^3 \frac{d^3 w_3(x_2)}{dx_2^3}\bigg|_{x_2=0} \tag{42}$$

Similarly, the continuity conditions for deflection and rotation at the interface of section 2 and section 4 are expressed as:

43

$$w_2(a) = w_4(0) \tag{43}$$

$$\left.\frac{dw_2(x_2)}{dx_2}\right|_{x_2=a} = \left.\frac{dw_4(x_4)}{dx_4}\right|_{x_4=0} \tag{44}$$

While those at the interface of section 3 and section 4 are expressed as:

$$w_3(a) = w_4(0) \tag{45}$$

$$\left.\frac{dw_3(x_2)}{dx_2}\right|_{x_2=a} = \left.\frac{dw_4(x_4)}{dx_4}\right|_{x_4=0} \tag{46}$$

Thus, the discontinuity of the moment and the continuity of the shear force at both the interface of section 4 and section 2 and the interface of section 4 and section 3 are expressed as follows by considering the expressions of Δp_1 in equation (9a):

$$\bar{t}^3 \left.\frac{d^2 w_2(x_2)}{dx_2^2}\right|_{x_2=a} + (1-\bar{t})^3 \left.\frac{d^2 w_3(x_2)}{dx_2^2}\right|_{x_2=a} - \frac{\beta(w_1'(L_1) - w_4'(0))}{3a}$$

$$= \left.\frac{d^2 w_4(x_4)}{dx_4^2}\right|_{x_4=0} \tag{47}$$

$$\bar{t}^3 \left.\frac{d^3 w_2(x_2)}{dx_2^3}\right|_{x_2=a} + (1-\bar{t})^3 \left.\frac{d^3 w_3(x_2)}{dx_2^3}\right|_{x_2=a} = \left.\frac{d^3 w_4(x_4)}{dx_4^3}\right|_{x_4=0} \tag{48}$$

Substitution of the expressions of $w_{1i}(x_1)$ $(i=1,2)$, $w_{4j}(x_4)$ $(j=1,3)$, $w_2(x_2)$ and $w_3(x_3)$ from equations (18), (19), (25), (26), (30) and (31) into the continuity and discontinuity conditions in Equations (34), (35), (36), (37), (40), (42), (43), (44), (45), (46), (47) and (48) leads to the

following homogeneous equation for the coefficients A_{1i}, A_{2i} $(i=1,2)$, B_1, B_2, B_3, B_4, C_1, C_2, C_3, C_4, D_{1j} and D_{2j} $(j=1,2,3)$:

$$[K] \begin{Bmatrix} A_{11} \\ A_{21} \\ B_1 \\ B_2 \\ B_3 \\ B_4 \\ C_1 \\ C_2 \\ C_3 \end{Bmatrix} = \begin{Bmatrix} 0 \\ 0 \\ 0 \\ 0 \\ 0 \\ 0 \\ 0 \\ 0 \\ 0 \end{Bmatrix} \tag{49}$$

where,

$[K]$ is the coefficient matrix.

The instability of the beam, that is, the buckling load for the delaminate beam will be derived from the condition for the non-trivial solution for A_{1i}, B_{2i} $(i=1,2)$, B_1, B_2, B_3, B_4, C_1, C_2, C_3, C_4, D_{1j} and D_{2j} $(j=1,2,3)$, from Equation (49) which is:

$$det \ [K] = 0 \tag{50}$$

The corresponding buckling mode shape is available from equations (18), (19), (25), (26), (30) and (31) after the buckling load F is derived. The process of deriving the buckling load and buckling mode shape involves the standard Eigen-value solution of equation (49).

Based on the above mechanics model, the buckling solutions for the two delaminated beams under investigation are obtained from the Eigen-value solutions of equation (49) using combinations of index (i,j) as follows:

- Simply supported beam (i=1, j=1)

- Cantilever beam (i=2, j=3)

3.4 Solution for repair of beams subjected to axial compression

Tensile and compressive forces are induced at the upper and lower layers of the delamination due to bending of the beams at their buckling modes. These induced forces lead to the sliding mode of fracture at the tips of delamination. Piezoelectric layers are used to induce counter shear forces at the interface of the piezoelectric layer and the host substrate by applying a suitable voltage. This helps avoid or control the sliding mode of fracture at the tip of the delamination, caused by action of axial compressive load and thus, renders the beam repaired.
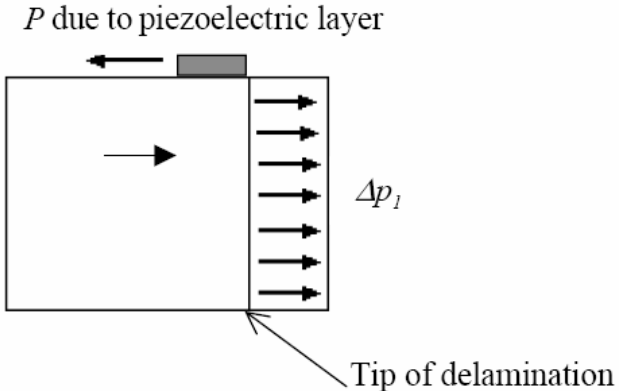
Figure 10: Upper layer of delamination bonded by piezoelectric patch
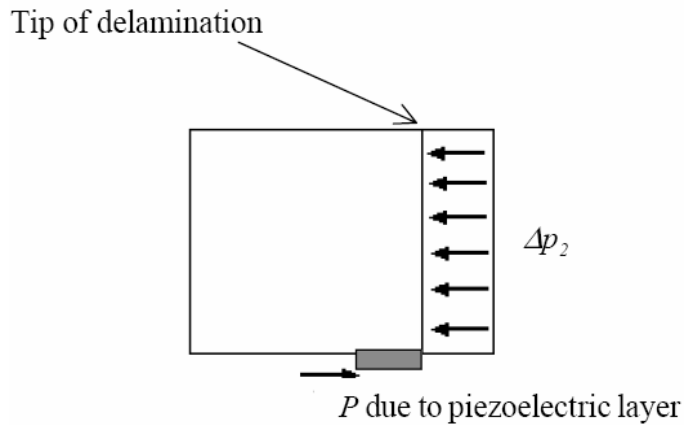
Figure 11: Lower layer of delamination bonded by piezoelectric patch

Figures 10 and 11 show free-body diagrams of the infinitesimal beam elements of the upper and lower layers of the delamination, surface-bonded by piezoelectric layers separately. It is easily seen that forces at the two layers of the piezoelectric actuators are essential to eliminate the tensile or compressive forces applied on the upper and lower layers of the delamination, due to the bending of the beam at the corresponding buckling mode. This helps erase the discontinuity of the shear forces at the tip of the delamination and thus the sliding mode of fracture can be avoided.

The first pair of piezoelectric actuators is to be bonded with their right ends in the vicinity of the left tip of the delamination, while the second pair is to be bonded with their left ends in the vicinity of the right tip of the delamination. It was indicated by Crawley and de Luis (1987) that the force transferred between the piezoelectric layer and the substrate is over an infinitesimal distance near the ends of the actuator, if an infinitely stiff bonding is provided. Therefore, it is reasonable to assume that the force induced by the piezoelectric layer is just over the

47

infinitesimal domain near the tip of the delamination, under perfect bonding. In other words, a thinner bonding layer and stiff bonding material is used.

It is expected that each pair of the piezoelectric layers will induce tensile and compressive forces of magnitude Δp_1, given by equation (9a), at the interfaces of the piezoelectric layers and the host beam as shown in Figures 10 and 11. Crawley and de Luis (1987) proposed the following expression for the shear force between a metal substrate and the piezoelectric layer, under the assumption of complete bonding between them:

$$P = \frac{EHT}{\psi + 6} \Lambda \tag{51}$$

with

$$\Psi = \frac{EH}{E_p h_1} \tag{52}$$

and

$$\Lambda = \frac{d_{31} V}{h_1} \tag{53}$$

where,

      h_1 – Thickness of the piezoelectric patch

      $\alpha = 6$, when structure is considered as a bar

      E_p – Equivalent Young's modulus of the piezoelectric layer for the one-

           dimensional problem

      d_{31} – Piezoelectric charge coefficient

Comparing equations (9a), (51), (52) and (53) and substituting $P = \Delta p1$ leads to the expression of the voltages applied to the pairs of the piezoelectric patches as follows:

$$V = \frac{h_1 \beta(\Psi + 6)}{2ad_{31}} \left(w'_L \Big|_{x=x_l} - w'_R \Big|_{x=x_r} \right) \tag{54}$$

Note that for each piezoelectric pair, the voltage at the upper and lower piezoelectric layers should be of the same magnitude but, should have different alignment in the poling direction of the piezoelectric layer, so that the forces in figure 12 can be induced.
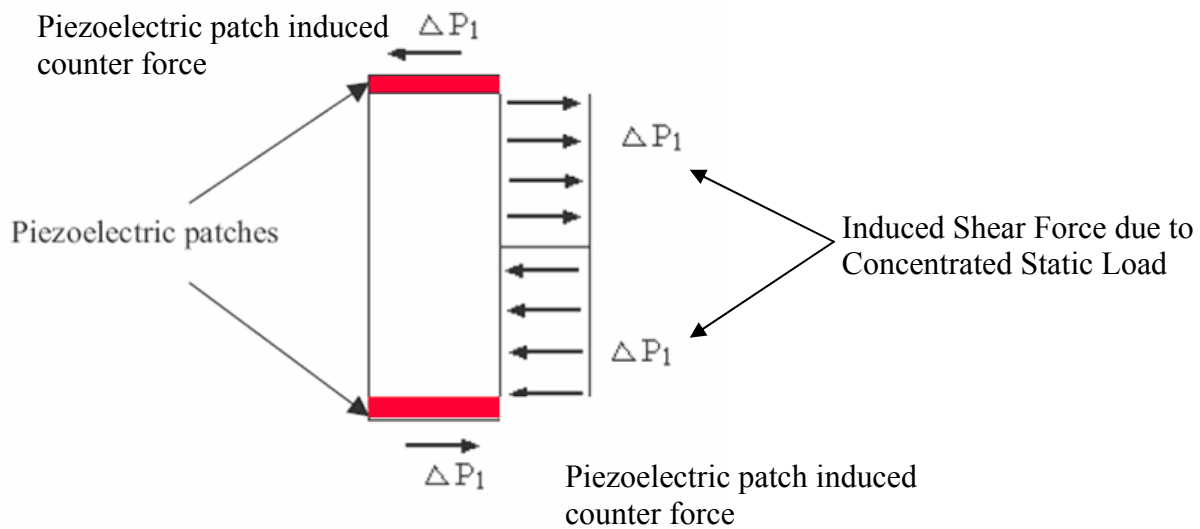

Figure 12: Repair of delamination by piezoelectric patches

It is seen that the induced forces by the piezoelectric pair will form a couple leading to a local bending to the beam structure. Such local bending definitely tends to induce deformation, but not singularity of stresses on the beam.

It is significant to note that the piezoelectric layers would be activated only if the measured deflection of the beam at a certain position, due to the buckling instability, exceeds a critical value of (*H/100*). Thus, the piezoelectric layer would only be "triggered" when a sensor signal is received and the voltage will be applied by a power amplifier to the piezoelectric layer, creating an active repair system. From equation (54), it is seen that the voltage applied on the piezoelectric patches is proportional to the difference of slope between left and right tips of delamination and is obtained from the Eigen-value solution of the equation (49).

3.5 Solution for repair of beams subjected to concentrated static load

As evident from the equation (54), the voltage applied on the piezoelectric patches is proportional to the difference in slope between the delamination tips. A sectional analysis is performed to derive the response of delaminated beams subjected to static loading for SS and CL boundary conditions. Due to continuity of deflection and slope at the delamination tips, it is reasonable to approximate the response of a delaminated beam to that of beam without delamination, on the condition that the effect of the delamination on the response of the delaminated beam is not obvious. This hypothesis is illustrated with a sectional analysis of a typical delaminated beam structure.
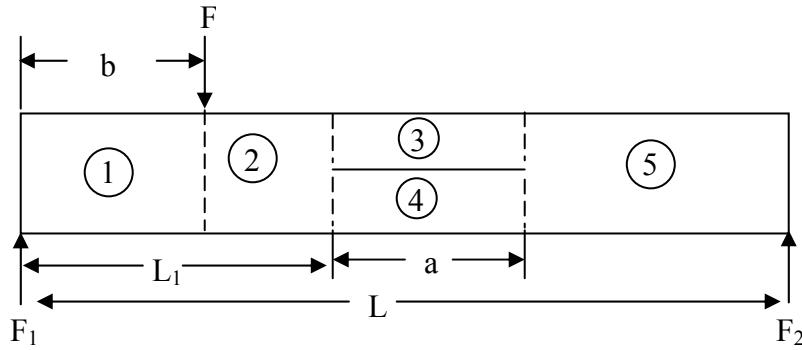
Figure 13: Sectional analysis of a delaminated beam

A delaminated beam shown in figure 13 is employed for the analysis. Denoting the support force at the left end as F_1, the force at the right end, F_2, is given as:

$$F_2 = F - F_1 \tag{55}$$

The moment induced at the right end is given by

$$M = F\left(L - b\right) - F_1 L \tag{56}$$

In context of figure 13, the three possible general cases of application of static load are:

Case-1: The static load is applied on the left side of the delamination.

That is, $b \leq L_1$

Case-2: The static load is applied between the two tips of delamination.

That is, $L_1 < b \leq (L_1 + a)$

Case-3: The static load is applied on the right side of the delamination.

That is, $b > (L_1 + a)$

where, b is the distance between line of action of force and left end of beam.

51

The expressions for response of the delaminated beam corresponding to the three static loading positions will be different. A detailed mechanics analysis for the case-1, when $b \leq L_1$, is considered hereinafter.

The beam is partitioned into five sections shown in figure 13. For section-1, the governing equation based on Euler–Bernoulli beam theory is:

$$EI \frac{d^2 y_1}{dx_1^2} = -M - F_1 x_1 \qquad for \quad \left(0 < x_1 < b\right) \qquad (57)$$

From equation (57), the solution of the deflection is obtained as:

$$y_1 = -\frac{F_1 x_1^3}{6EI} - \frac{M x_1^2}{2EI} + y_1'(0) x_1 + y_1(0) \qquad (58)$$

where,

$y_1(0)$ and $y_1'(0)$ are boundary conditions at the left end of the beam.

The governing equation for section-2 is:

$$EI \frac{d^2 y_2}{dx_2^2} = \left(F - F_1\right) x_2 - \left(F - F_1\right)\left(L - b\right) \qquad for \quad \left(0 < x_2 < \left(L_1 - b\right)\right) \qquad (59)$$

which has a general solution given by:

$$y_2 = \frac{\left(F - F_1\right) x_2^3}{6EI} - \frac{\left(F - F_1\right)\left(L - b\right) x_2^2}{2EI} + b_1 x_2 + b_2 \qquad (60)$$

where,

$$b_1 = -\frac{1}{2EI} F_1 b^2 - \frac{Mb}{EI} + y_1'(0) \qquad (61)$$

$$b_2 = -\frac{1}{6EI}F_1 b^3 - \frac{M}{2EI}b^2 + y_1'(0)b + y_1(0) \tag{62}$$

Based on the continuity conditions at $x_1 = b$ and $x_2 = 0$, we have,

$$y_1 = y_2 \tag{63}$$

and

$$y_1' = y_2' \tag{64}$$

From equation (60), the slope at the left tip of the delamination is expressed as

$$y_2' = \frac{\left(F - F_1\right)\left(L_1-b\right)^2}{2EI} - \frac{\left(F - F_1\right)\left(L - b\right)\left(L_1-b\right)}{EI} + b_1 \tag{65}$$

Equation (65) is a function of only one unknown parameter, F_1, and the boundary conditions at the left end of the beam. The reaction force at the left end of the beam is independent of the delamination, for the cases of SS and CL beams.

The slope at the right tip of delamination can be obtained similarly. Hence, the expressions for the slopes for beams with no delamination are related to the derivation of the voltage applied to the piezoelectric patches, for the repair of delaminated beams.
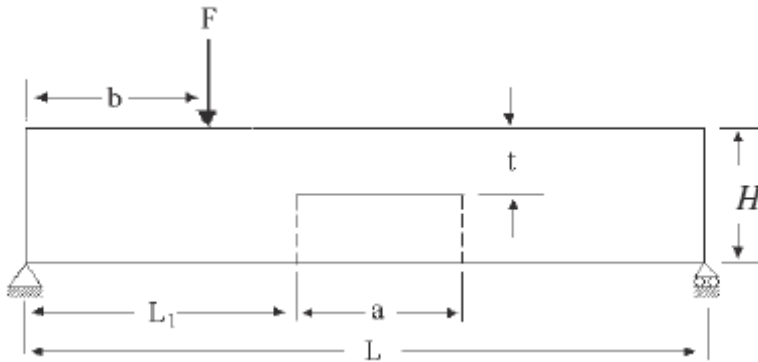
Figure 14: Delaminated SS beam
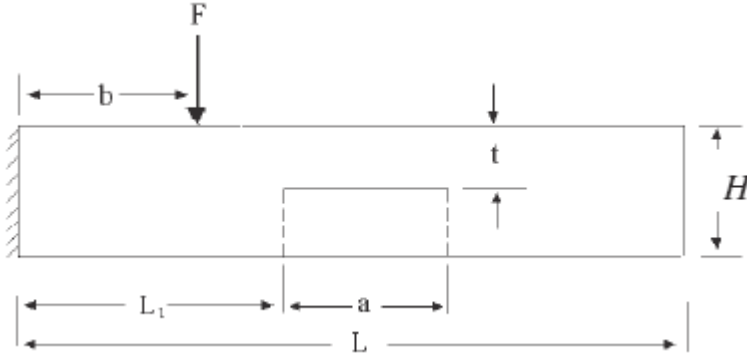
Figure 15: Delaminated CL beam

The responses of the slopes for SS and CL beams shown in figures 14 and 15 are quoted from the book by Gere (2001), and the solutions for the voltage are listed as follows:

For SS beam:

Case-1: $b \leq L_1$

$$w_L'\Big|_{x=x_L} - w_R'\Big|_{x=x_R} = -\frac{Fb}{LEI}\left(a\,(L-L_1)-\frac{a^2}{2}\right) \tag{66}$$

$$V = \frac{Fb\,h_1\,\beta\,(\Psi+6)}{2L\,d_{31}\,EI}\left((L-L_1)-\frac{a}{2}\right) \tag{67}$$

Case-2: $L_1 < b \leq (L_1+a)$

$$w_L'\Big|_{x=x_L} - w_R'\Big|_{x=x_R} = -\frac{F(L-b)}{6LEI}\left(2Lb-b^2-3L_1^2\right)-\frac{Fb}{6LEI}\left(L^2-b^2-3(L-a-L_1)^2\right) \tag{68}$$

$$V = \frac{F\,h_1\,\beta\,(\Psi+6)}{12La\,d_{31}\,EI}\left((L-b)\left(2Lb-b^2-3L_1^2\right)+b\left(L^2-b^2-3(L-a-L_1)^2\right)\right) \tag{69}$$

Case-3: $b > (L_1+a)$

$$w_L'\Big|_{x=x_L} - w_R'\Big|_{x=x_R} = -\frac{F(L-b)}{LEI}\left(aL_1+\frac{a^2}{2}\right) \tag{70}$$

$$V = \frac{F\,(L-b)\,h_1\,\beta\,(\Psi+6)}{2Ld_{31}\,EI}\left(L_1+\frac{a}{2}\right) \tag{71}$$

For CL beam:

Case-1: $b \leq L_1$

$$w'_L\big|_{x=x_L} - w'_R\big|_{x=x_R} = 0 \tag{72}$$

$$V = 0 \tag{73}$$

Case-2: $L_1 < b \leq (L_1+a)$

$$w'_L\big|_{x=x_L} - w'_R\big|_{x=x_R} = -\frac{F}{2EI}\left(2bL_1 - L_1^2 + b^2\right) \tag{74}$$

$$V = \frac{F\,h_1\,\beta(\Psi+6)}{4a d_{31}EI}\left(2bL_1 - L_1^2 + b^2\right) \tag{75}$$

Case-3: $b > (L_1+a)$

$$w'_L\big|_{x=x_L} - w'_R\big|_{x=x_R} = -\frac{F}{2EI}\left(-2ba + a^2 + 2aL_1\right) \tag{76}$$

$$V = \frac{F\,h_1\,\beta(\Psi+6)}{4d_{31}EI}\left(-2b + a + 2L_1\right) \tag{77}$$

CHAPTER-4: NUMERICAL SIMULATIONS

4.1 Simulation Parameters

Numerical simulations are conducted to estimate the repair voltage for cases of delaminated SS and CL beams, based on the theory proposed by Wang and Quek (2004) and Wang, Zhou and Quek (2005). The various simulation parameters considered for the beams and piezoelectric patches are as follows:

$L = 1m$

$T = 0.05m$

$H = 0.01m$

$E = (210 \times 10^9) \, Nm^{-2}$

$E_p = (63 \times 10^9) \, Nm^{-2}$

$h_1 = 0.001m$

$d_{31} = (190 \times 10^{-12}) \, mV^{-1}$

Since the magnitudes of the voltages applied on all the piezoelectric patches are the same, we only investigate the variation of the voltage inducing compression in the piezoelectric layers. An estimate of repair voltage for following two cases of external loads is provided:

- Concentrated static load
- Axial compression load

4.2 Repair of delaminated beams subjected to concentrated static load

Current section provides a discussion on the numerical simulations for the case of delaminated SS and CL beams.

4.2.1 SS beams

Variation of the repair voltage against different parameters can be conveniently derived using equations 67, 69 and 71.

The voltage to be applied on the piezoelectric patches for the various values of L_1, the distance between the left delamination tip and left end of the beam, is listed in Table 1, at t=0.005m, b=0.5m, a=0.2m and F=1N. The results show that the repair voltage is larger as we approach the center of the beam, and is found to have maximum value at the center of the beam. Figure 16 shows the variation of repair voltage plotted for different values of L_1.

Table 1: NS of repair voltage on piezoelectric layers for different values of L_1, for a SS beam subjected to concentrated static load

L_1 (m)	Repair Voltage V (volts)
0.1	29.5739
0.2	44.3609
0.3	59.1479
0.4	66.5414
0.5	59.1479
0.6	44.3609
0.7	29.5739
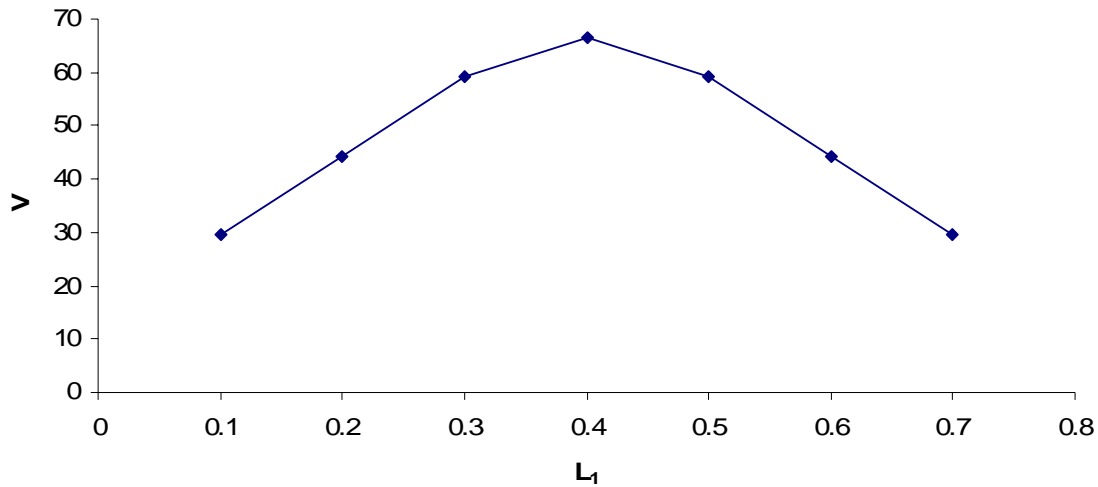
Figure 16: NS of (V vs. L_1), for a SS beam subjected to concentrated static load

The repair voltage is found to show a similar variation for different values of b, the location of the force along the longitudinal direction of the beam. Table 2 lists the repair voltage for different values of b, at a=0.2m, L1=0.4m and t=0.005m, under the action of F=1N. The results show that larger voltages will be needed if the force is applied at the center of the beam. On the other hand, no voltage is necessary if the force is applied at the ends of the beam. This observation is obvious due to the fact that V=0 at b=0 or L, as seen from the equations 67, 69 and 71. Figure 17 shows the variation of repair voltage versus b.

Table 2: NS of repair voltage on piezoelectric layers for different values of b, for a SS beam subjected to concentrated static load

b (m)	Repair Voltage V (volts)
0.0	00.0000
0.1	14.7870
0.2	29.5739
0.3	44.3609
0.4	59.1479
0.5	66.5414
0.6	59.1479
0.7	44.3609
0.8	29.5739
0.9	14.7870
1.0	00.0000
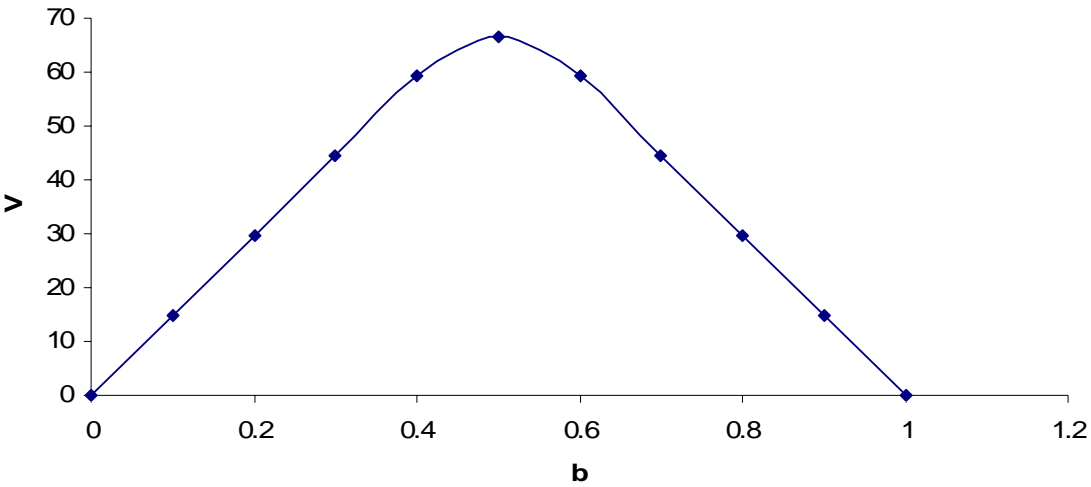
Figure 17: NS of (V vs. b), for a SS beam subjected to concentrated static load

Figure 18 shows the variation of the repair voltage plotted against the length of the delamination (a), at L_1=0.4m, b=0.5m, t=0.005m and F=1N. The magnitude of the repair voltage is found to decrease with increase in the size of delamination. This can be easily verified from the equation

69. Table 3 lists the values of repair voltage on the piezoelectric patches for different values of

the delamination length.

Table 3: NS of repair voltage on piezoelectric layers for different values of a, for a SS beam

subjected to concentrated static load

a (m)	Repair Voltage V (volts)
0.2	66.5414
0.3	61.6124
0.4	55.4511
0.5	48.7970
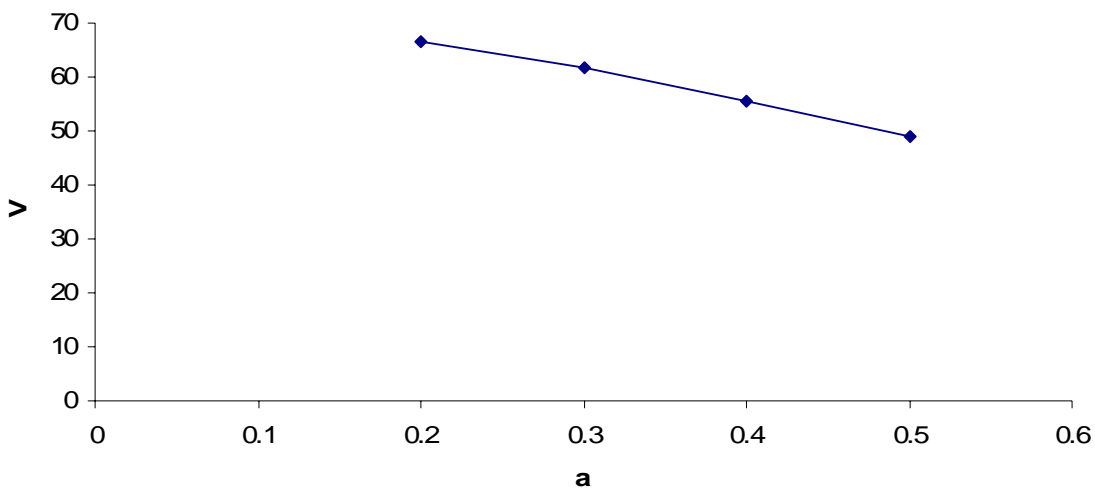
Figure 18: NS of (V vs. a) for a SS beam subjected to concentrated static load

4.2.2 CL beams

In case of the CL beams, variation of the repair voltage against different parameters is obtained from the equations 73, 75 and 77.

The voltage to be applied on the piezoelectric patches for the various values of L_1 is listed in Table 4, at a=0.2m, b=0.5m, t=0.005m and F=1N. Figure 19 shows a plot of variation of repair voltage based on the values in Table 4. As seen from the figure, the repair voltage for $L_1 \geq 0.5$m is zero. This is obvious from equation 73 where, for $L_1 \geq 0.5$m, b$\leq L_1$ always.

Table 4: NS of repair voltage on piezoelectric layers for different values of L_1, for a CL beam subjected to concentrated static load

L_1 (m)	Repair Voltage V (volts)
0.1	-88.7218
0.2	-59.1479
0.3	340.1003
0.4	362.2807
0.5	0
0.6	0
0.7	0
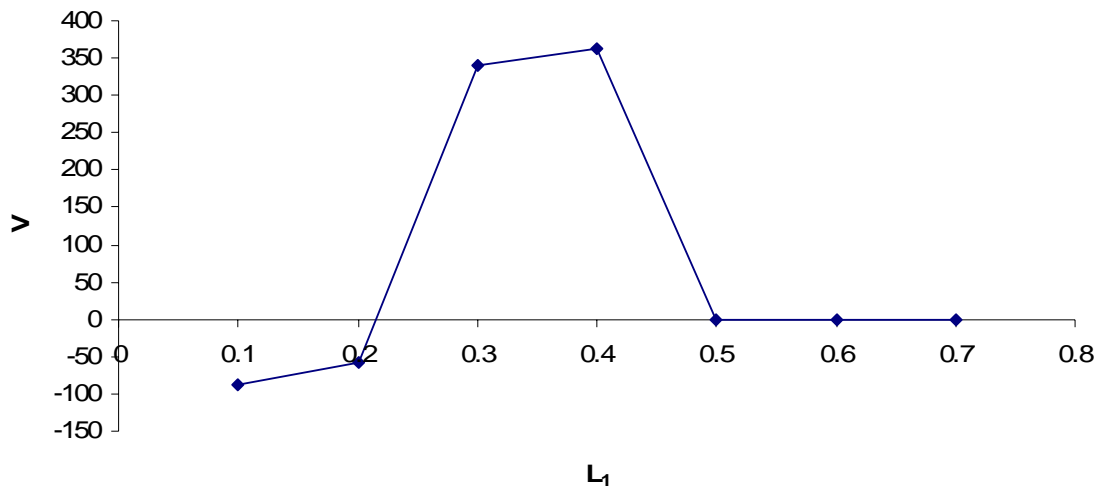
Figure 19: NS of (V vs. L_1), for a CL beam subjected to concentrated static load

Table 5 lists the values of the repair voltage applied on the piezoelectric patches for the different values of the loading location, b, at 4, at a=0.2m, L_1=0.4m, t=0.005m and F=1N. Values in Table 5 are plotted in Figure 20, which shows that the repair voltage for b≤0.4m is zero. This is again obvious from equation 73.

Table 5: NS of repair voltage on piezoelectric layers for different values of **b**, for a CL beam

subjected to concentrated static load

b (m)	Repair Voltage V (volts)
0.1	0
0.2	0
0.3	0
0.4	0
0.5	362.2807
0.6	502.7569
0.7	-59.1479
0.8	-88.7218
0.9	-118.296
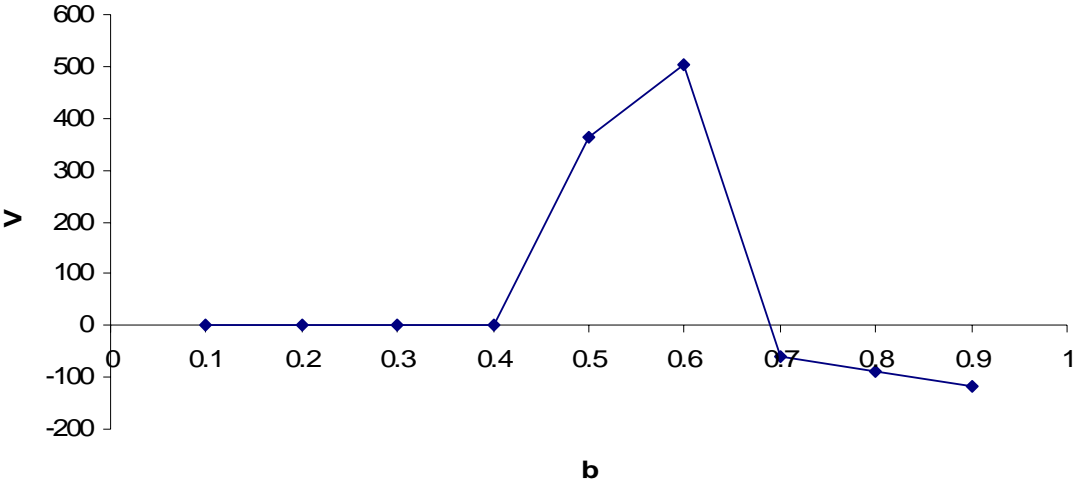
Figure 20: NS of (V vs. b), for a CL beam subjected to concentrated static load

On the basis of values in Table 6, variation of the repair voltage is plotted for different values of the size of delamination (a) in Figure 21. Calculations are conducted using equations 73, 75 and 77, at L_1=0.1m, b=0.5m, t=0.005m and F=1N. As seen from the figure, the magnitude of the repair voltage decreases with increase in the size of delamination, as in equation 75.

Table 6: NS of repair voltage on piezoelectric layers for different values of **a**, for a CL beam subjected to concentrated static load

a (m)	Repair Voltage V (volts)
0.4	125.6892
0.5	100.5514
0.6	83.7928
0.7	71.8224
0.8	62.8446
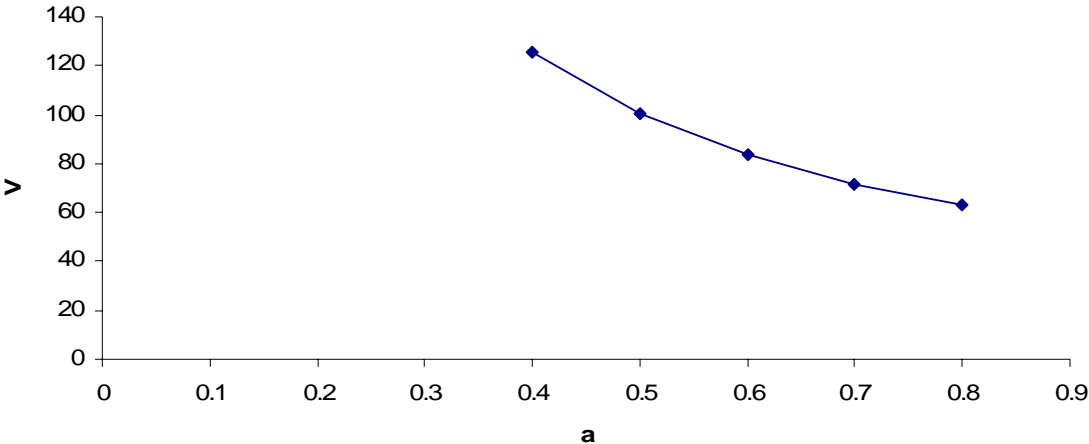
Figure 21: NS of (V vs. a), for a CL beam subjected to concentrated static load

4.3 Repair of delaminated beams subjected to axial compression load

Current section provides a discussion on the numerical simulations for the case of delaminated SS and CL beams by the way of non-dimensional analysis. The non-dimensional parameters used in the simulations are:

Length of the delamination, $\bar{a} = \dfrac{a}{L}$

Distance of the delamination to the left end of the beam, $\bar{L}_1 = \dfrac{L1}{L}$

Distance of the delamination to the top of the beam, $\bar{t} = \dfrac{t}{H}$

The non-dimensional buckling load is defined as $\bar{F} = \dfrac{F}{F_{cr}}$

where,

F_{cr} is the buckling load for the healthy beam. For example, the buckling load of a healthy SS beam (Timoshenko and Gere, 1961) is given by:

$$F_{cr} = \frac{\pi^2 EI}{L^2}$$

while that of a healthy CL beam (Timoshenko and Gere, 1961) is given by:

$$F_{cr} = \frac{\pi^2 EI}{4L^2}$$

In all subsequent simulations, the value of the voltage is derived by assuming that the piezoelectric layer would only be activated if the measured deflection of the beam at its center due to the buckling instability reaches a critical value of *H / 100*. Distribution pattern of the repair voltage obtained here serves as a basis or guideline for similar distribution pattern for different values of deflection. Simulation results are based on the Eigen value solution of the equation 49 and equations 51 and 54.

4.3.1 SS beams

The voltage required on the piezoelectric layer, to erase the sliding mode of fracture for a delaminated SS beam, is plotted in Figure 22. The horizontal axis in the figure is the location of the center of the delamination. It is seen that the maximum voltage is required when the delamination is located around the center of the beam.

This observation can be explained from Equation 54 which shows that the required voltage is proportional to the difference of the slope between the two tips of the delamination, i.e. the average curvature on the span of the delamination. Since the curvature of the buckling mode of a simply supported beam is the maximum at the center, it is reasonable to see from Figure 22 that the maximum voltage is required when the delamination is located at the center of the beam. Table 7 shows the values of the repair voltage required for corresponding value of location of the center of delamination.

Table 7: NS of repair voltage on piezoelectric layers for different values of center of

delamination, for a SS beam subjected to axial compression

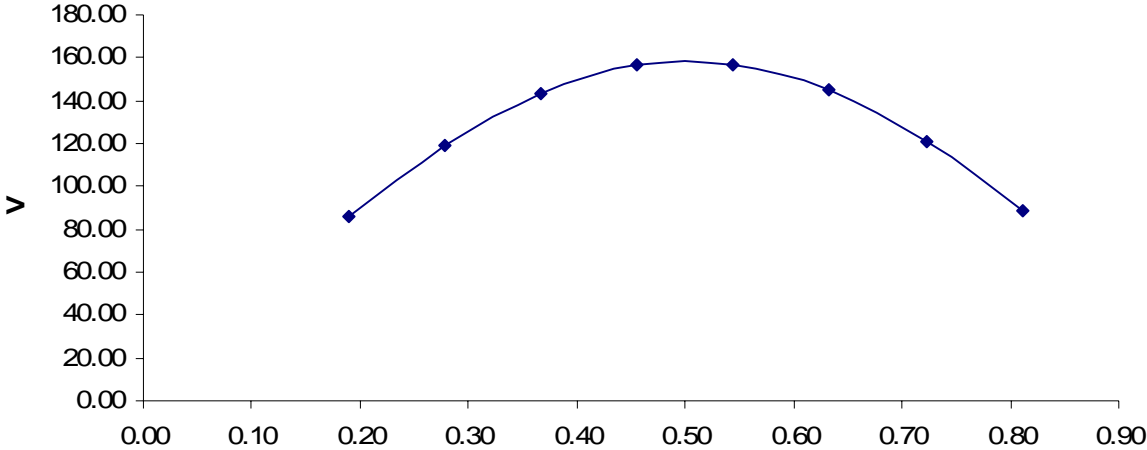| Center of Delamination (m)	Repair Voltage V (volts)
0.19	85.83
0.28	119.41
0.37	143.69
0.46	156.70
0.54	156.98
0.63	144.70
0.72	121.30
0.81	89.01

Figure 22: NS of (V vs. Center of Delamination), for a SS beam subjected to axial compression

4.3.2 CL beams

Table 8 lists the values of the repair voltage required for various values of location of the center of delamination. The required voltage on the piezoelectric layer for the cantilever beam is plotted in Figure 23, against the center of delamination. It is seen that from the figure that the maximum voltage is required if the delamination is located at the fixed end of the beam while, a minimum voltage is required if the delamination is around the free end of the beam.

Table 8: NS of repair voltage on piezoelectric layers for different values of center of delamination, for a CL beam subjected to axial compression

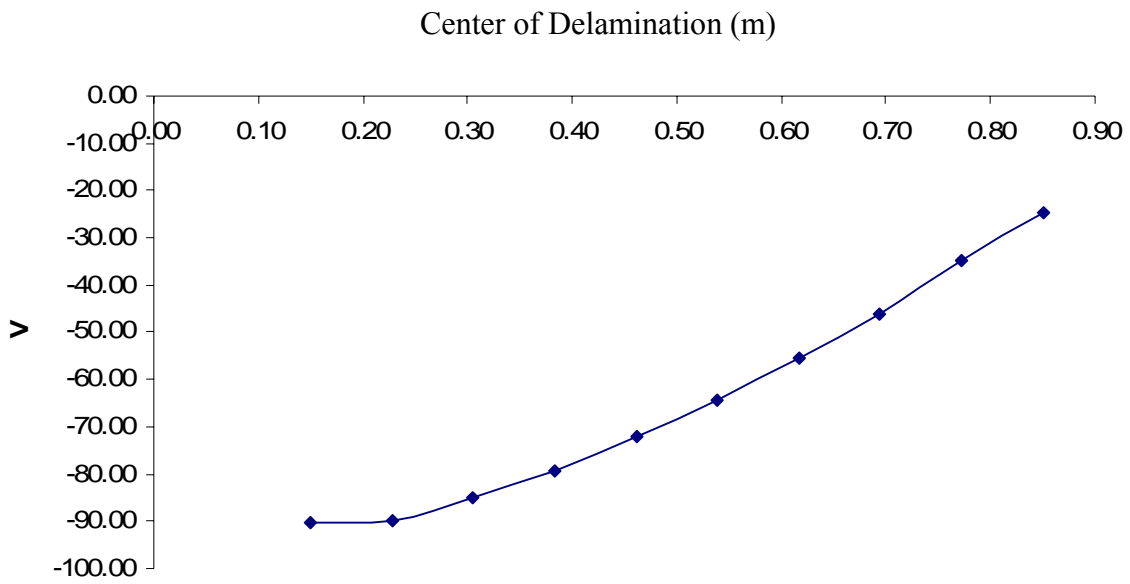| Center of Delamination (m)	Repair Voltage V (volts)
0.15	-90.33
0.23	-89.75
0.31	-85.17
0.38	-79.30
0.46	-72.22
0.54	-64.29
0.62	-55.33
0.69	-46.13
0.77	-34.92
0.85	-24.82

Center of Delamination (m)

Figure 23: NS of (V vs. Center of Delamination), for a CL beam subjected to axial compression

CHAPTER 5: FINITE ELEMENT SIMULATION

FE simulations provide powerful tool to create a virtual model of the real world applications from various disciplines like solids, fluids and structures. Numerical FE packages, with different capabilities and applications, are available these days viz., IDEAS, ANSYS, ABAQUS, Pro-Mechanica, etc. The underlying principle behind FE simulations remains same to a greater or lesser extent, in all these packages. The process of FE analysis or simulations involves three basic stages:

1) Pre-processing – It involves creating a CAD/geometric model of the part, creating and assigning material and physical properties to individual parts, creating assembly of the parts, generating a mesh and applying the required constraints, loads and boundary conditions. Results are governed by the type of elements used and the quality of mesh generated. The basic unknown parameter here is the nodal displacement.

2) Processing – It involves the stiffness generation, mass generation, stiffness modification and solution of equations resulting in the evaluation of the nodal variables. Other derived quantities such as gradients or stresses may be evaluated at this stage too. A stiffness and mass matrix are formed for all the elements and are assembled to obtain the corresponding global matrices. These are then modified by applying the boundary conditions. The nodal displacements are calculated by solving the FE equations and subsequent stresses and strains.

3) Post-processing – It involves extraction of the results from the FE analysis. In case a static analysis it involves estimation of displacements and stresses, and for bucking

analysis it involves estimation of mode shapes, Eigen-values and frequencies of vibration for the structure.

Of the various FE packages available, ABAQUS was selected to perform the FE simulations in current work, due to its capabilities

- to model delamination

- to simulate piezoelectric material properties

The version 6.4 of ABAQUS was used for perform all the subsequent simulations.

5.1 FE simulation using ABAQUS

FE simulations using ABAQUS/CAE involves the use of modules, and performing the corresponding stated tasks, in the sequence mentioned in the Table 9.

Table 9: Simulation steps in ABAQUS v6.4
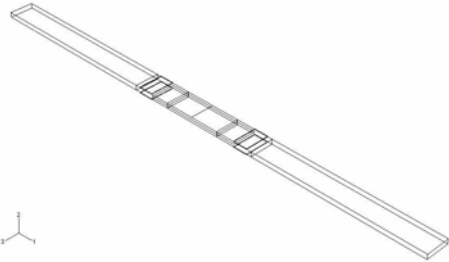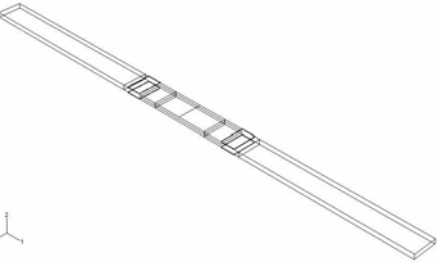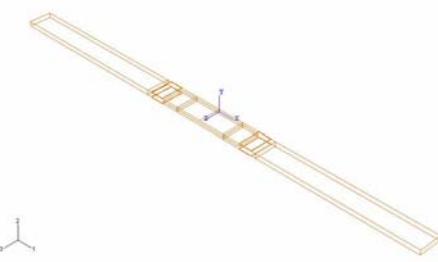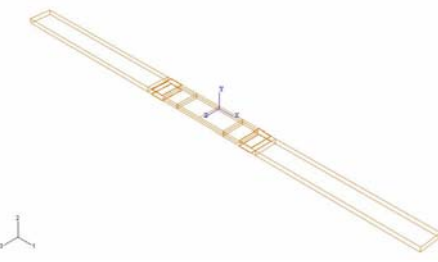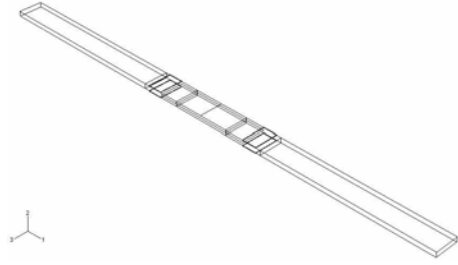
Step #	Module Name / FE analysis Stage	Task/s	Model at End of Task/s
1	Part / Pre-processing	Create a part with features • Delaminated beam • Four Piezoelectric patches surface mounted on the beam	
2	Property / Pre-processing	• Define the materials for beam and piezoelectric patch • Create distinct sections for beam and patches • Assign sections to beam and piezoelectric patches	
3	Assembly / Pre-processing	Create an instance of the part in step-1	
4	Step / Pre-processing	• Define the nature of analysis viz., General-Static or Linear Perturbation-Buckle, with Subspace Eigen-solver • Define the outputs desired	

Table 9: Simulation steps in ABAQUS v6.4 (contd.)

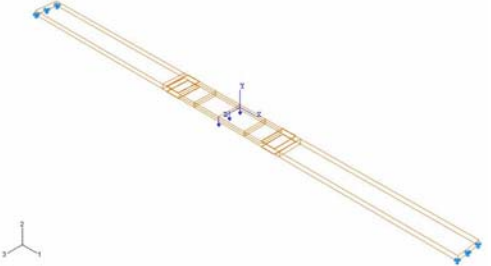| Step #	Module Name / FE analysis Stage	Task/s	Model at End of Task/s
5	Load / Pre-processing	Define the loads and BCs. BCs need to be defined for both, the beam and the piezoelectric patches	
6	Mesh / Pre-processing	• Define and assign the elements used for different features in the model; C3D6H for beam while, C3D6E for piezoelectric patch • Define the desired distribution of elements along various features/sub-sections in model • Generate a mesh	
7	Job / Processing	• Create a job to be analyzed • Perform analysis	
8	Visualization / Post-processing	• Create a display group which includes features of interest (delamination in our case) • View results	

5.2 Simulation Parameters

This section validates the results proposed in 'Chapter 4: Numerical Simulations' using FE

simulations, and thus, employs the same material and geometric parameters used by the various

corresponding sections in Chapter 4. In addition to the parameters used for conducting NS, some

additional parameters required for conducting the FE simulations are as follows:

Poisson's ratio for beam material: 0.29

Density of beam material: 7850 kgm^{-3}

Poisson's ratio for piezoelectric patch: 0.33

Density for piezoelectric materials: 1514 kgm^{-3}

Piezoelectric coupling matrix:

$$
\begin{bmatrix}
15.080 & 0.0 & 0.0 \\
-5.207 & 0.0 & 0.0 \\
-5.207 & 0.0 & 0.0 \\
0.0 & 12.710 & 0.0
\end{bmatrix}
\text{Coulomb m}^{-2}
$$

FE simulations are conducted to validate the repair voltage for cases of delaminated SS and CL

beams subjected to the following two cases of external loads:

- Concentrated static load
- Axial compression load

5.3 Validation of repair voltage for delaminated beams subjected to concentrated static load

In this section the results proposed in various sub-sections of section 4.2 are validated.

5.3.1 SS beams

In this section, a discussion is provided on results from FE simulations performed for the case of a delaminated SS beam subjected to concentrated static load.

Tables 10, 11 and 12 list the variation of repair voltage obtained from FE simulations for different values of L_1, b and a respectively. The values in Tables 10, 11 and 12 are obtained for (t=0.005m, b=0.5m, a=0.2m and F=1N), (a=0.2m, L1=0.4m, t=0.005m and F=1N) and (L_1=0.4m, b=0.5m, t=0.005m and F=1N) respectively.

Figures 24, 26 and 28 show the distribution of repair voltage plotted against L_1, b and a respectively, being based on Tables 10, 11 and 12 respectively. The distribution pattern in Figures 24, 26 and 28 is found to be similar to that in Figures 16, 17 and 18, which is based on NS.

Figures 25, 27 and 29 show the singularity of stresses at delamination tips, before and after application of repair voltage.

Table 10: FE simulated repair voltage on piezoelectric layers for different values of L_1, for a SS beam subjected to concentrated static load

L_1 (m)	Repair Voltage V (volts)
0.1	26
0.2	40
0.3	53
0.4	59
0.5	49
0.6	38
0.7	25

Figure 24: FE simulation of (V vs. L_1), for a SS beam subjected to concentrated static load

(a) Before application of repair voltage

(b) After application of repair voltage

Figure 25: Singularity of stresses at delamination tips for a SS beam at L_1=0.1m

Table 11: FE simulated repair voltage on piezoelectric layers for different values of b, for a SS beam subjected to concentrated static load

b (m)	Repair Voltage V (volts)
0	0
0.1	11
0.2	26
0.3	38
0.4	52
0.5	59
0.6	49
0.7	40
0.8	25
0.9	10
1	0

Figure 26: FE simulation of (V vs. b), for a SS beam subjected to concentrated static load

(a) Before application of repair voltage

(b) After application of repair voltage

Figure 27: Singularity of stresses at delamination tips for a SS beam at b=0.9m

Table 12: FE simulated repair voltage on piezoelectric layers for different values of a, for a SS

beam subjected to concentrated static load

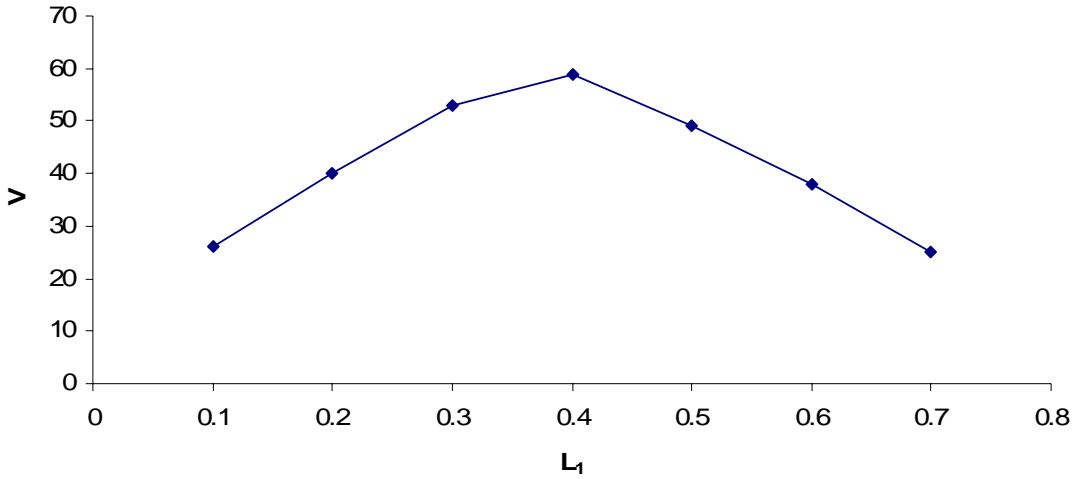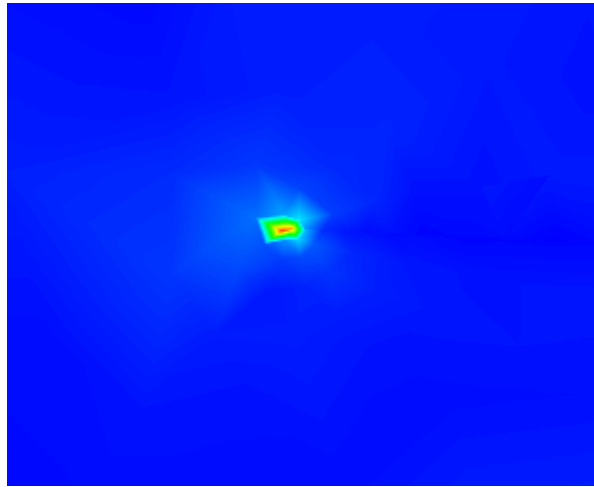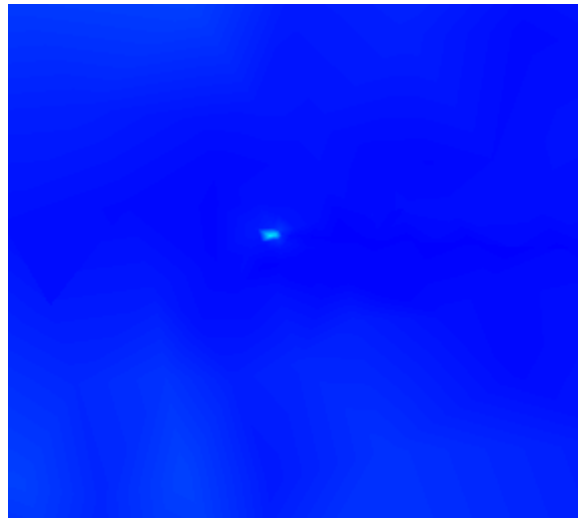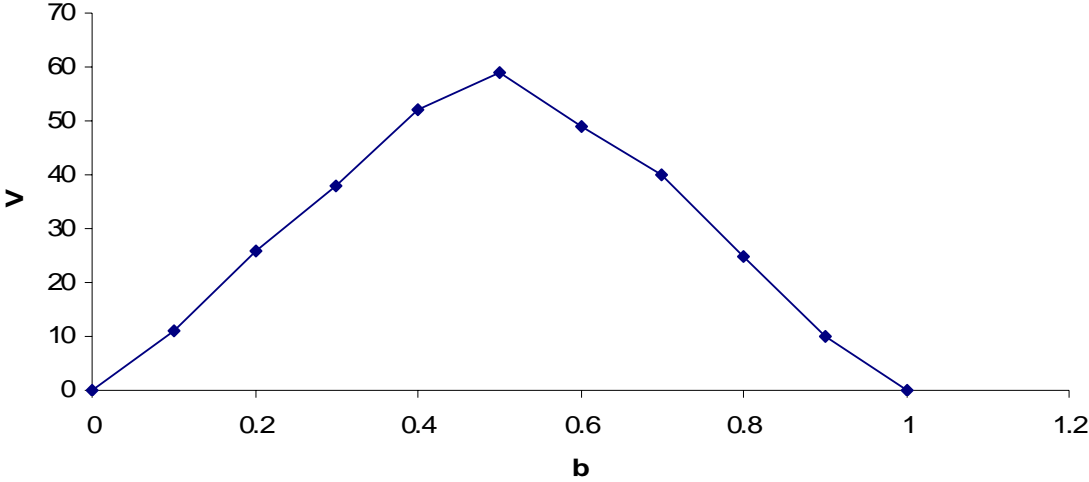| a (m)	Repair Voltage V (volts)
0.2	59
0.3	51
0.4	47
0.5	43

Figure 28: FE simulation of (V vs. a) for a SS beam subjected to concentrated static load

(a) Before application of repair voltage

(b) After application of repair voltage

Figure 29: Singularity of stresses at delamination tips for a SS beam at a=0.2m

5.3.2 CL beams

This section discusses the results from FE simulations performed for the case of a delaminated CL beam subjected to concentrated static load.

Tables 13, 14 and 15 list the variation of repair voltage obtained from FE simulations for different values of the parameters L_1, b and a respectively. The values in Tables 13, 14 and 15 are obtained for (t=0.005m, b=0.5m, a=0.2m and F=1N), (a=0.2m, L1=0.4m, t=0.005m and F=1N) and (L_1=0.4m, b=0.5m, t=0.005m and F=1N) respectively.

Figures 30, 32 and 34 show the distribution of repair voltage plotted against the parameters L_1, b and a respectively, based on Tables 13, 14 and 15 respectively. The distribution pattern in Figures 30, 32 and 34 follows the one similar to in Figures 19, 20 and 21, which is based on NS.

Figures 31, 33 and 35 show the singularity of stresses at the tips of delamination, before and after application of repair voltage.

Table 13: FE simulated repair voltage on piezoelectric layers for different values of L_1, for a CL

beam subjected to concentrated static load

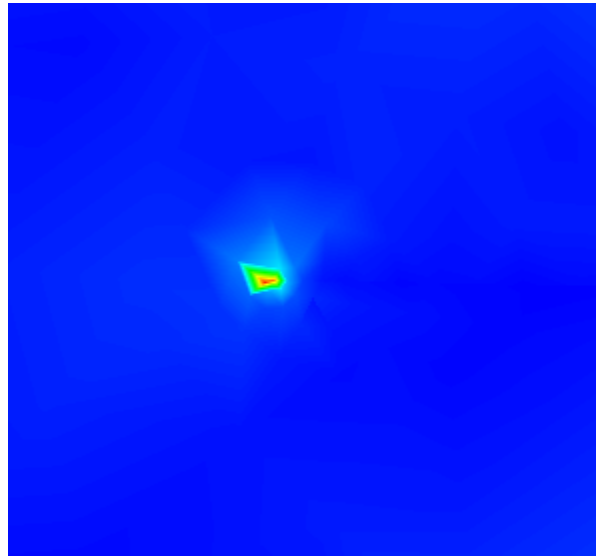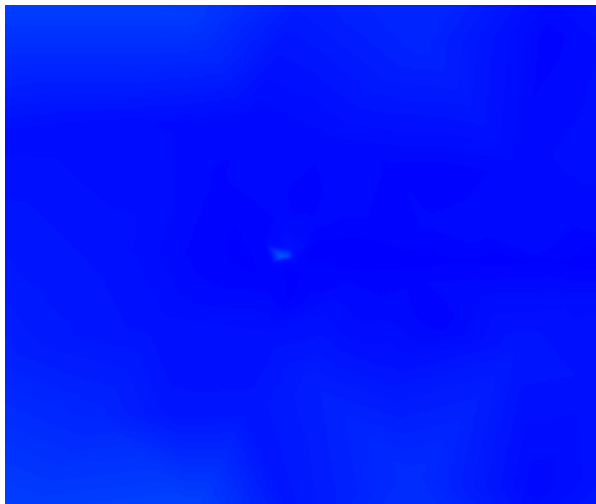| L1 (m)	Repair Voltage V (volts)
0.1	-95
0.2	-70
0.3	320
0.4	350
0.5	0
0.6	0
0.7	0
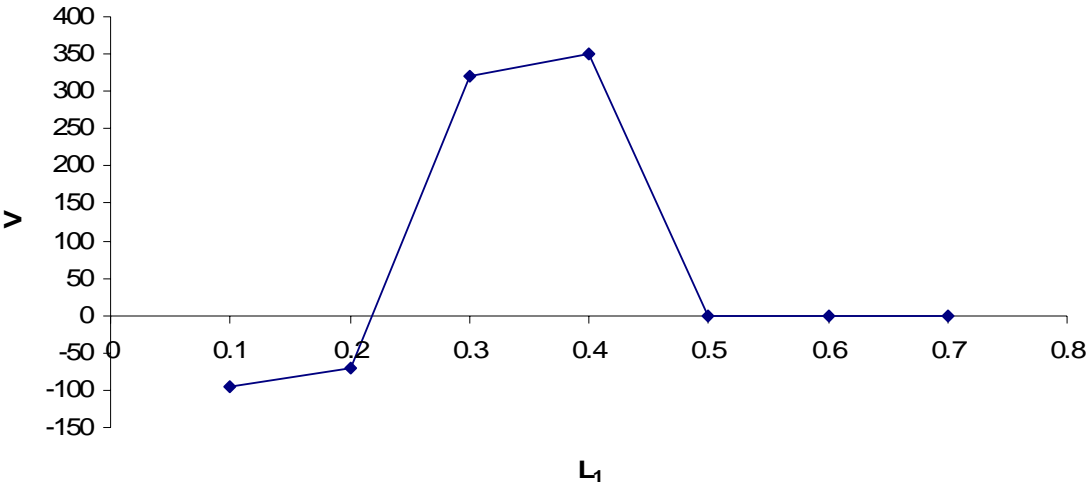
Figure 30: FE simulation of (V vs. L_1), for a CL beam subjected to concentrated static load
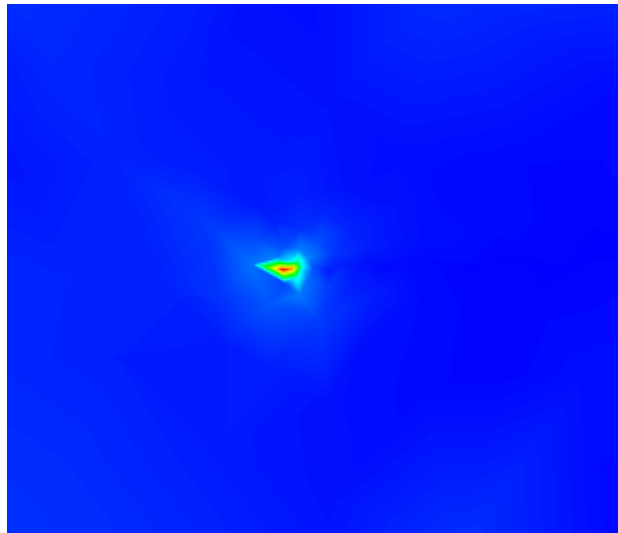
(a) Before application of repair voltage
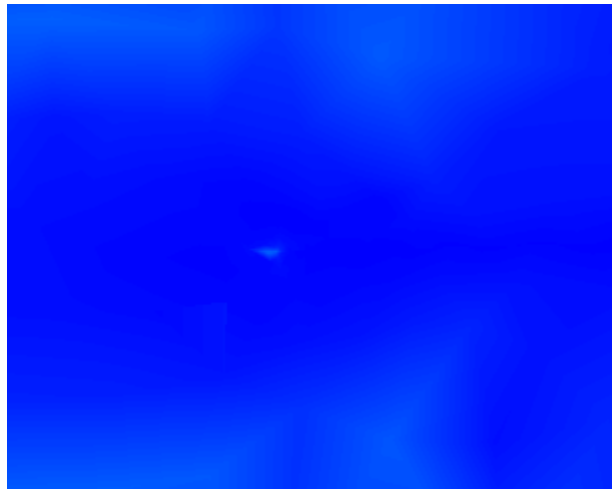
(b) After application of repair voltage

Figure 31: Singularity of stresses at delamination tips for a CL beam at L1=0.1m

Table 14: FE simulated repair voltage on piezoelectric layers for different values of **b**, for a CL

beam subjected to concentrated static load

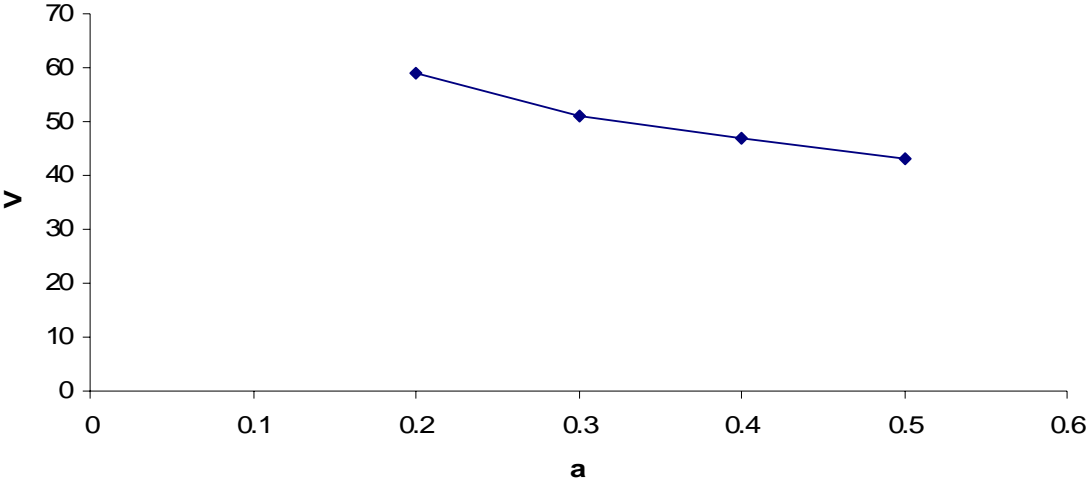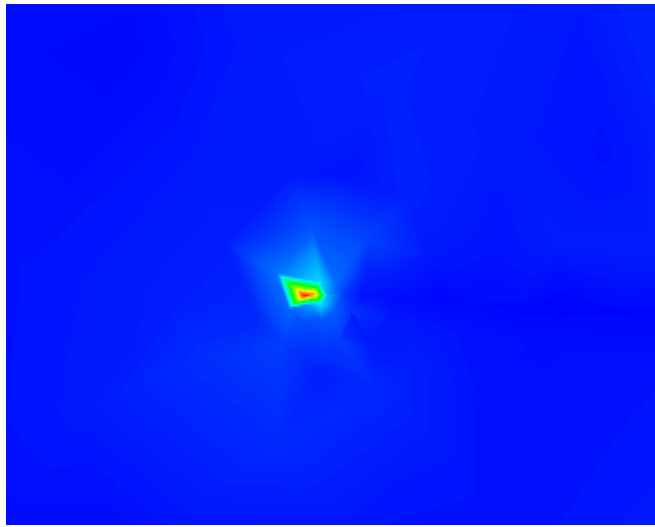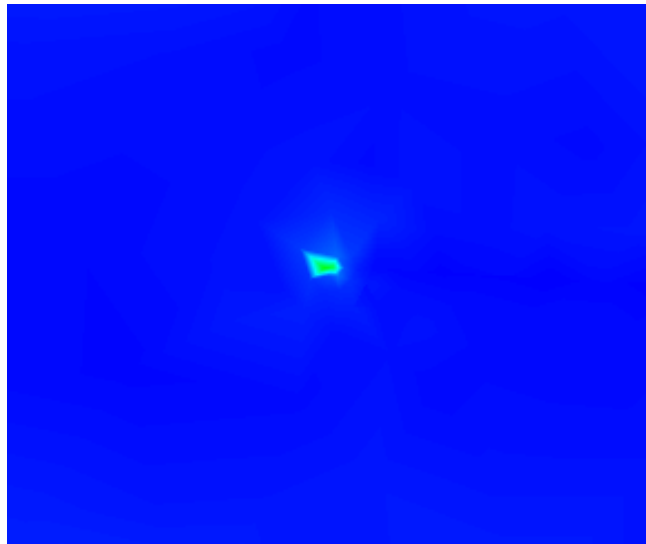| b (m)	Repair Voltage V (volts)
0.1	0
0.2	0
0.3	0
0.4	0
0.5	345
0.6	475
0.7	-67
0.8	-95
0.9	-125
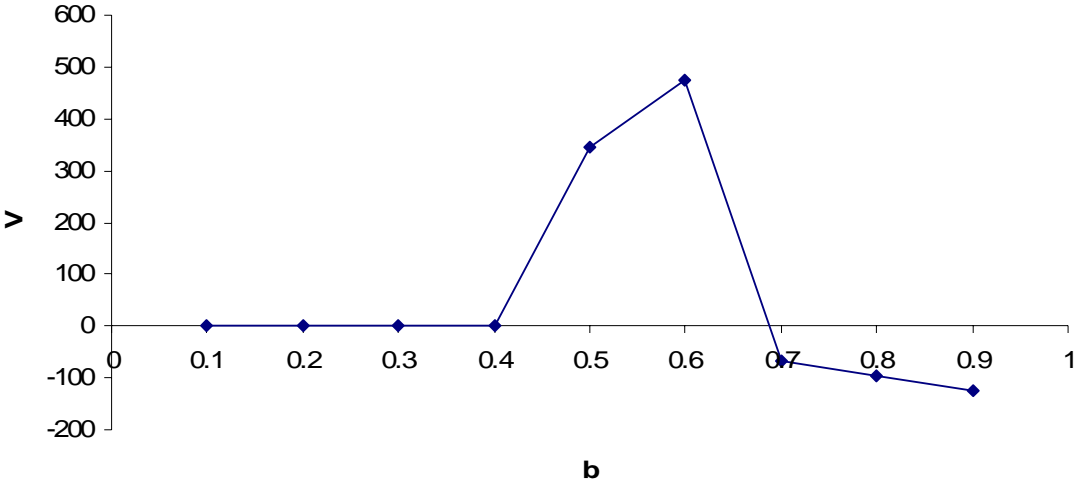
Figure 32: FE simulation of (V vs. b), for a CL beam subjected to concentrated static load
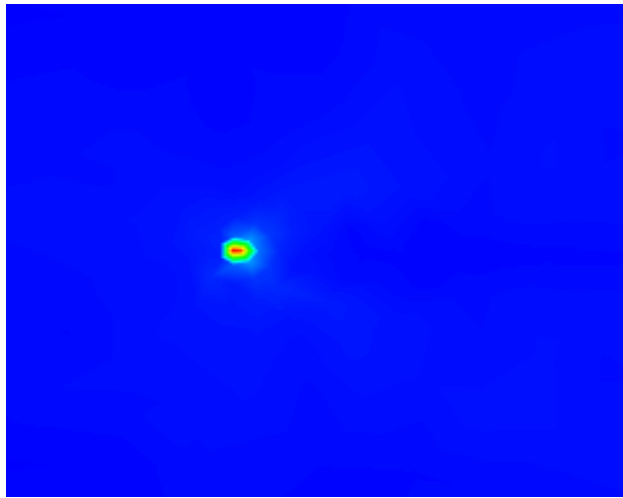
(a) Before application of repair voltage
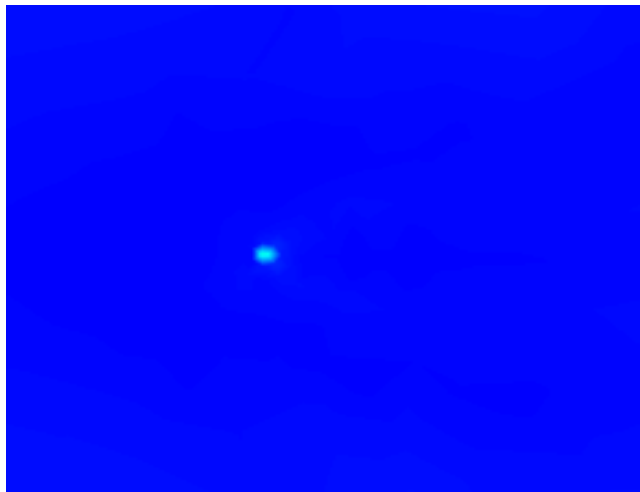
(b) After application of repair voltage

Figure 33: Singularity of stresses at delamination tips for a CL beam at b=0.8m

Table 15: FE simulated repair voltage on piezoelectric layers for different values of **a**, for a CL

beam subjected to concentrated static load

a (m)	Repair Voltage V (volts)
0.4	115
0.5	97
0.6	75
0.7	67
0.8	61
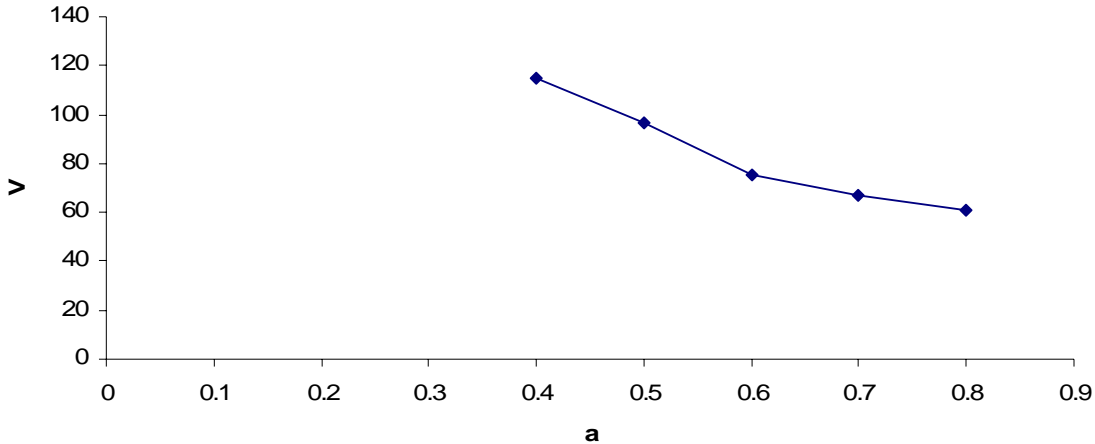
Figure 34: FE simulation of (V vs. a), for a CL beam subjected to concentrated static load
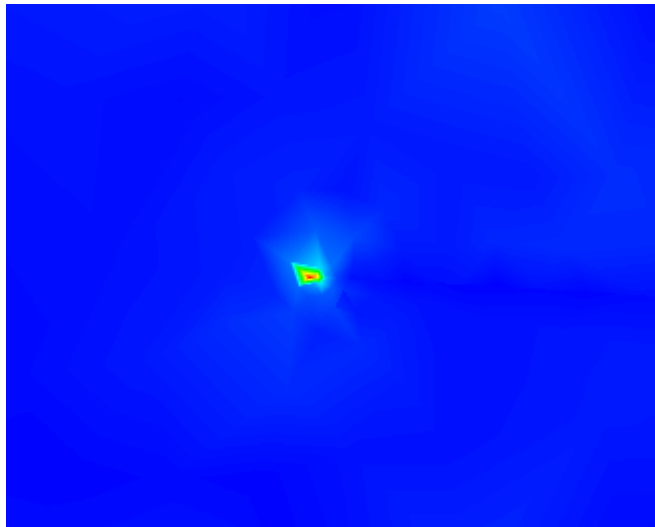
(a) Before application of repair voltage
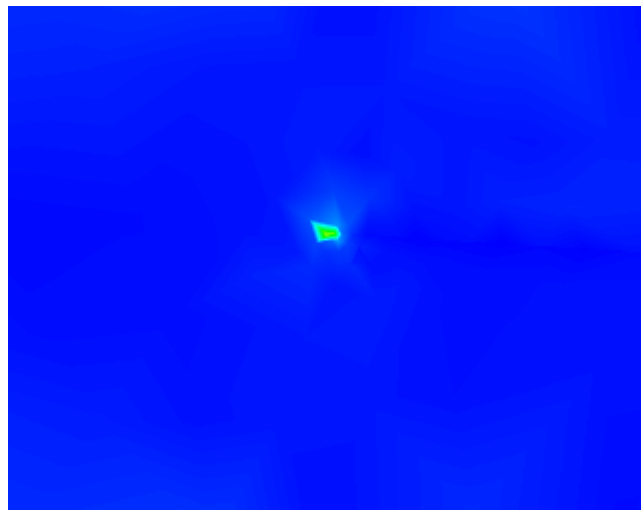
(b) After application of repair voltage

Figure 35: Singularity of stresses at delamination tips for a CL beam at a =0.5m

5.4 Repair of delaminated beams subjected to axial compression load

This section discusses the results from FE simulations performed for the case of a delaminated SS and CL beam subjected to axial compression load.

5.4.1 SS beams

Table 16 lists the variation of repair voltage obtained from FE simulations for different values of the center of delamination. The values in Tables 16 are obtained for t=0.005m, b=0.5m, a=0.2m. Figure 36 shows distribution of repair voltage plotted against the values of center of delamination in Tables 16. The distribution pattern in Figures 36 is found to be similar to that in Figure 22, based on NS.

Figure 37 shows the singularity of stresses at delamination tips, before and after application of repair voltage.

Table 16: FE simulated repair voltage on piezoelectric layers for different values of center of delamination, for a SS beam subjected to axial compression

Center of Delamination (m)	Repair Voltage V (volts)
0.2	98.00
0.3	127.00
0.4	151.00
0.5	167.00
0.6	168.00
0.7	154.00
0.8	129.00

Figure 36: FE simulation of (V vs. Center of Delamination), for a SS beam subjected to axial compression
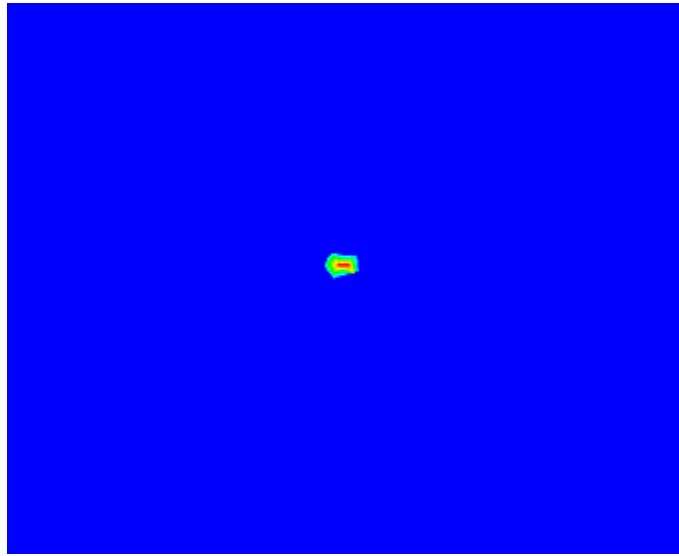
(a) Before application of repair voltage
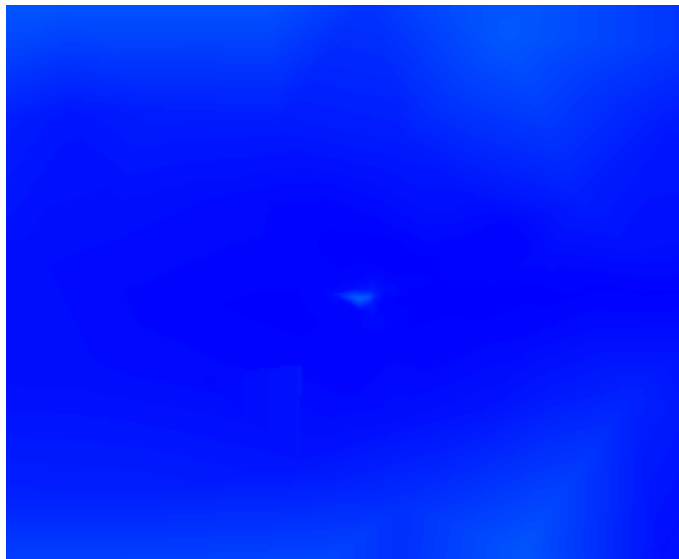
(b) After application of repair voltage

Figure 37: Singularity of stresses at delamination tips for a SS beam for Distance of center of delamination from left end of beam as 0.3m

5.4.2 CL beams

Table 17 lists the variation of repair voltage obtained from FE simulations for different values of the center of delamination. The values in Tables 17 are obtained for t=0.005m, b=0.5m, a=0.2m. Figure 38 shows distribution of repair voltage plotted against the values of center of delamination in Tables 17. The distribution pattern in Figures 38 is found to be similar to that in Figure 23, based on NS.

Figure 39 shows the singularity of stresses at delamination tips, before and after application of repair voltage.

Table 17: FE simulated repair voltage on piezoelectric layers for different values of center of

delamination, for a CL beam subjected to axial compression

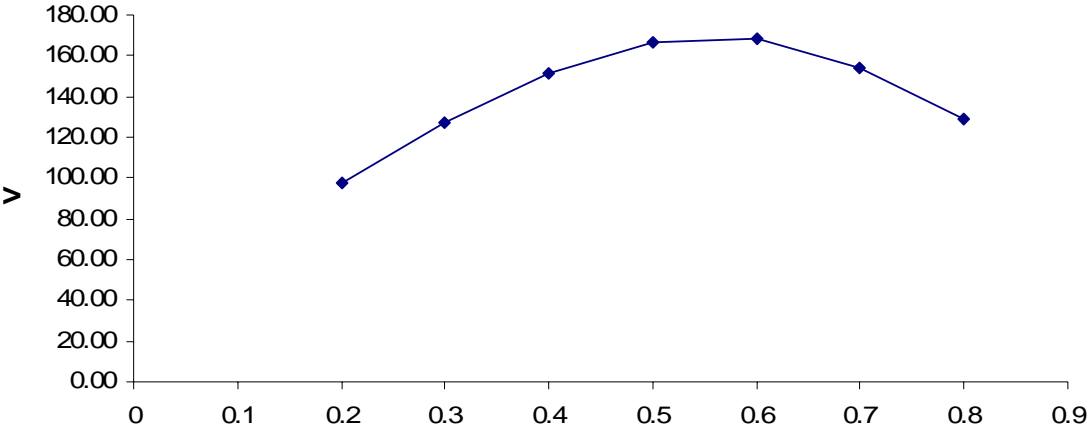| Center of Delamination (m)	Repair Voltage V (volts)
0.2	-97.00
0.3	-97.00
0.4	-93.00
0.5	-85.00
0.6	-74.00
0.7	-55.00
0.8	-51.00
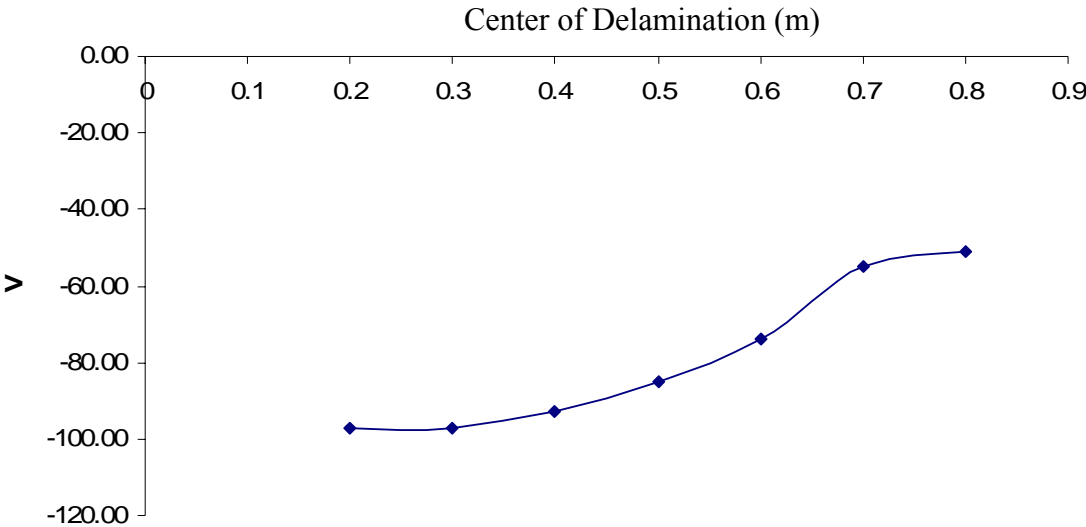
Figure 38: FE simulation of (V vs. Center of Delamination), for a CL beam subjected to axial

compression
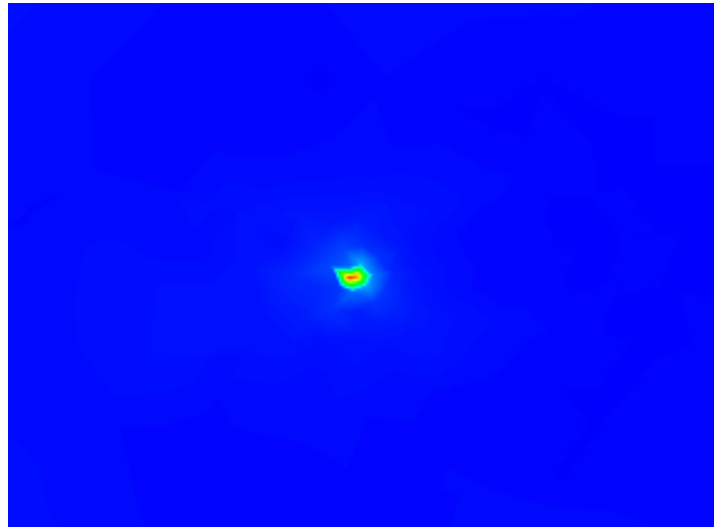
(a) Before application of repair voltage
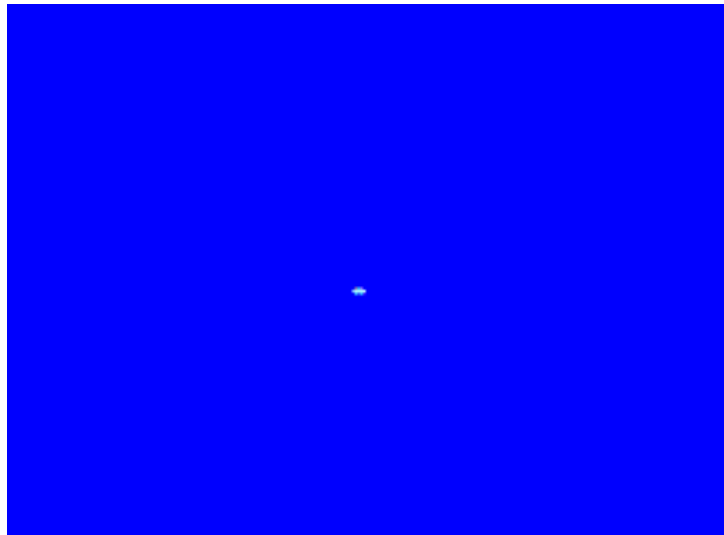
(b) After application of repair voltage

Figure 39: Singularity of stresses at delamination tips for a CL beam for Distance of center of delamination from left end of beam as 0.3m

CHAPTER 6: CONCLUSION

During the course of this work, the effect of delamination on composite structures was studied considering relatively simple examples of SS and CL beams subjected to concentrated static load and axial compression loads. The delamination in beam structures is found to induce discontinuity of shear stresses at its tips, and is among the primary causes of failure of the beam structures. The use of the electromechanical characteristics of piezoelectric materials for repair of delaminated composite structures was considered through various sections of this work.

A detailed mechanics analysis of delaminated beams, subjected to concentrated static load and axial compression load, was provided and numerical simulations were performed to calculate the repair voltage to be applied to the piezoelectric layers. Under the action of repair voltage on piezoelectric layers, the discontinuity of the shear stress at the tips of delamination is eliminated, and the beam is thus repaired. The variation of repair voltage with location and size of the delamination was also considered. Subsequently, a validation study was performed to confirm the numerically proposed values of repair voltage by the way of FE simulations using the CAD tool ABAQUS v6.4.

The research presented is an example of the relatively simpler actuator models for the application of smart materials in composite repair. It provides the necessary information for the design of piezoelectric materials for repair of delaminated composites. It also provides a solid foundation for the application of smart materials based on more advanced models like, coupled actuator-sensor models, coupled electromechanical models and coupled thermoelectromechanical models.

APPENDIX A: CONSTITUTIVE RELATIONSHIPS OF PIEZOELECTRIC MATERIAL

The piezoelectric material is a kind of transverse isotropic material. In planes normal to the poling direction, all directions are equivalent with respect to the material properties. For plane problems, plate problems and beam problems, the respective 2-D or 1-D constitutive relationships may need to be derived from the 3-D constitutive relationship. Without losing arbitrariness, a coordinate system is supposed so that the thickness directions of plates and beams are in the axis 3, the longitudinal direction of beam is in axis 1, as shown in Figure A 1: and Figure A 2.
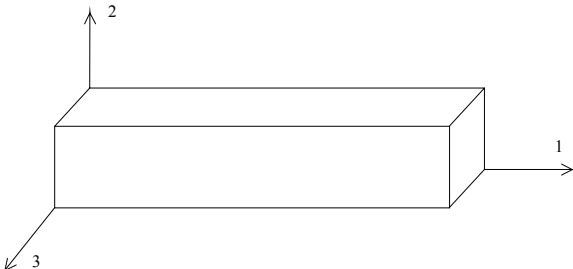
Figure A 1: Beam
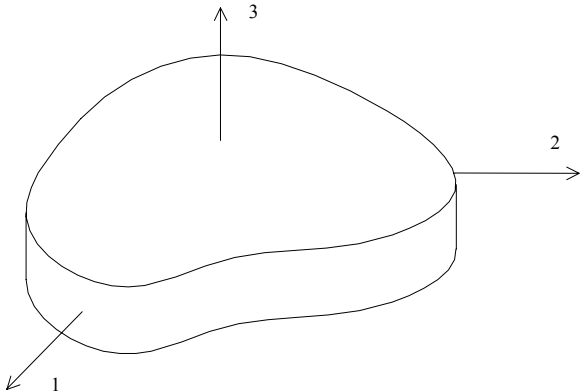
Figure A 2: Plate

A.1 Poling Direction in Axis 3

If the piezoelectric material is poled in the direction 3, its constitutive relationship is given by

$$
\begin{Bmatrix} \sigma_{11} \\ \sigma_{22} \\ \sigma_{33} \\ \sigma_{12} \\ \sigma_{13} \\ \sigma_{23} \end{Bmatrix} =
\begin{pmatrix}
C_{11}^E & C_{12}^E & C_{13}^E & 0 & 0 & 0 \\
C_{12}^E & C_{11}^E & C_{13}^E & 0 & 0 & 0 \\
C_{13}^E & C_{13}^E & C_{33}^E & 0 & 0 & 0 \\
0 & 0 & 0 & \frac{1}{2}(C_{11}^E - C_{12}^E) & 0 & 0 \\
0 & 0 & 0 & 0 & C_{55}^E & 0 \\
0 & 0 & 0 & 0 & 0 & C_{55}^E
\end{pmatrix}
\begin{Bmatrix} \varepsilon_{11} \\ \varepsilon_{22} \\ \varepsilon_{33} \\ \gamma_{12} \\ \gamma_{13} \\ \gamma_{23} \end{Bmatrix}
$$
$$
-\begin{pmatrix}
0 & 0 & e_{31} \\
0 & 0 & e_{31} \\
0 & 0 & e_{33} \\
0 & 0 & 0 \\
e_{15} & 0 & 0 \\
0 & e_{15} & 0
\end{pmatrix}
\begin{Bmatrix} E_1 \\ E_2 \\ E_3 \end{Bmatrix},
\qquad \text{(A-1)}
$$

$$
\begin{Bmatrix} D_1 \\ D_2 \\ D_3 \end{Bmatrix} =
\begin{pmatrix}
0 & 0 & 0 & 0 & e_{15} & 0 \\
0 & 0 & 0 & 0 & 0 & e_{15} \\
e_{31} & e_{31} & e_{33} & 0 & 0 & 0
\end{pmatrix}
\begin{Bmatrix} \varepsilon_{11} \\ \varepsilon_{22} \\ \varepsilon_{33} \\ \gamma_{12} \\ \gamma_{13} \\ \gamma_{23} \end{Bmatrix}
+
\begin{pmatrix}
\Xi_{11} & 0 & 0 \\
0 & \Xi_{11} & 0 \\
0 & 0 & \Xi_{33}
\end{pmatrix}
\begin{Bmatrix} E_1 \\ E_2 \\ E_3 \end{Bmatrix},
\qquad \text{(A-2)}
$$

where σ_{11}, σ_{22}, σ_{33}, σ_{12}, σ_{13}, and σ_{23} are the stress components; ε_{11}, ε_{22}, ε_{33}, γ_{12}, γ_{13}, and γ_{23} the engineering strain components; D_1, D_2, and D_3 the electric displacements; E_1, E_2, and E_3 the electric field intensities; C_{11}^E, C_{33}^E, C_{12}^E, C_{13}^E, and C_{55}^E the elasticity moduli at constant electric field; e_{31}, e_{33}, and e_{15} the piezoelectric strain coefficients; Ξ_{11}, and Ξ_{33} the dielectric constants.

(1) For the Mindlin's Plate Model (IPT)

Solving $\sigma_{33} = 0$ for $\varepsilon_{33} = 0$ gives

$$\varepsilon_{33} = \frac{e_{33}}{C_{33}^E} E_3 - \frac{C_{13}^E}{C_{33}^E}(\varepsilon_{11} + \varepsilon_{22}) \tag{A-3}$$

Substituting equation (A-3) into equations (A-1) and (A-2) yields

$$
\begin{Bmatrix} \sigma_{11} \\ \sigma_{22} \\ \sigma_{12} \\ \sigma_{13} \\ \sigma_{23} \end{Bmatrix} =
\begin{pmatrix}
\overline{C}_{11}^E & \overline{C}_{12}^E & 0 & 0 & 0 \\
\overline{C}_{12}^E & \overline{C}_{11}^E & 0 & 0 & 0 \\
0 & 0 & \frac{1}{2}(\overline{C}_{11}^E - \overline{C}_{12}^E) & 0 & 0 \\
0 & 0 & 0 & C_{55}^E & 0 \\
0 & 0 & 0 & 0 & C_{55}^E
\end{pmatrix}
\begin{Bmatrix} \varepsilon_{11} \\ \varepsilon_{22} \\ \gamma_{12} \\ \gamma_{13} \\ \gamma_{23} \end{Bmatrix}
-
\begin{pmatrix}
0 & 0 & \overline{e}_{31} \\
0 & 0 & \overline{e}_{31} \\
0 & 0 & 0 \\
e_{15} & 0 & 0 \\
0 & e_{15} & 0
\end{pmatrix}
\begin{Bmatrix} E_1 \\ E_2 \\ E_3 \end{Bmatrix}
\tag{A-4}
$$

$$
\begin{Bmatrix} D_1 \\ D_2 \\ D_3 \end{Bmatrix} =
\begin{pmatrix}
0 & 0 & 0 & e_{15} & 0 \\
0 & 0 & 0 & 0 & e_{15} \\
\overline{e}_{31} & \overline{e}_{31} & 0 & 0 & 0
\end{pmatrix}
\begin{Bmatrix} \varepsilon_{11} \\ \varepsilon_{22} \\ \gamma_{12} \\ \gamma_{13} \\ \gamma_{23} \end{Bmatrix}
+
\begin{pmatrix}
\Xi_{11} & 0 & 0 \\
0 & \Xi_{11} & 0 \\
0 & 0 & \overline{\overline{\Xi}}_{33}
\end{pmatrix}
\begin{Bmatrix} E_1 \\ E_2 \\ E_3 \end{Bmatrix}
\tag{A-5}
$$

where $\overline{C}_{11}^E$, $\overline{C}_{12}^E$, $\overline{e}_{31}$, and $\overline{\overline{\Xi}}_{33}$ are given by

$$\overline{C}_{11}^E = C_{11}^E - \frac{(C_{13}^E)^2}{C_{33}^E}, \qquad \overline{C}_{12}^E = C_{12}^E - \frac{(C_{13}^E)^2}{C_{33}^E},$$

$$\tag{A-6}$$

$$\overline{e}_{31} = e_{31} - \frac{C_{13}^E}{C_{33}^E} e_{33}, \qquad \overline{\overline{\Xi}}_{33} = \Xi_{33} + \frac{e_{33}^2}{C_{33}^E}.$$

If the transverse shear stiffness is modified by a shear factor κ^2, equation (A-4) becomes

$$
\begin{Bmatrix} \sigma_{11} \\ \sigma_{22} \\ \sigma_{12} \\ \sigma_{13} \\ \sigma_{23} \end{Bmatrix} = \begin{pmatrix} \overline{C}^E_{11} & \overline{C}^E_{12} & 0 & 0 & 0 \\ \overline{C}^E_{12} & \overline{C}^E_{11} & 0 & 0 & 0 \\ 0 & 0 & \frac{1}{2}(\overline{C}^E_{11} - \overline{C}^E_{12}) & 0 & 0 \\ 0 & 0 & 0 & \kappa^2 C^E_{55} & 0 \\ 0 & 0 & 0 & 0 & \kappa^2 C^E_{55} \end{pmatrix} \begin{Bmatrix} \varepsilon_{11} \\ \varepsilon_{22} \\ \gamma_{12} \\ \gamma_{13} \\ \gamma_{23} \end{Bmatrix}
$$

$$
- \begin{pmatrix} 0 & 0 & \overline{e}_{31} \\ 0 & 0 & \overline{e}_{31} \\ 0 & 0 & 0 \\ e_{15} & 0 & 0 \\ 0 & e_{15} & 0 \end{pmatrix} \begin{Bmatrix} E_1 \\ E_2 \\ E_3 \end{Bmatrix}.
$$

(A-7)

(2) For the Kirchhoff's Plate Model (CPT)

Omitting the last two equations of (A-4) yields

$$
\begin{Bmatrix} \sigma_{11} \\ \sigma_{22} \\ \sigma_{12} \end{Bmatrix} = \begin{pmatrix} \overline{C}^E_{11} & \overline{C}^E_{12} & 0 \\ \overline{C}^E_{12} & \overline{C}^E_{11} & 0 \\ 0 & 0 & \frac{1}{2}(\overline{C}^E_{11} - \overline{C}^E_{12}) \end{pmatrix} \begin{Bmatrix} \varepsilon_{11} \\ \varepsilon_{22} \\ \gamma_{12} \end{Bmatrix} - \begin{pmatrix} 0 & 0 & \overline{e}_{31} \\ 0 & 0 & \overline{e}_{31} \\ 0 & 0 & 0 \end{pmatrix} \begin{Bmatrix} E_1 \\ E_2 \\ E_3 \end{Bmatrix}
$$

(A-8)

Besides of $\sigma_{33} = 0$ the CPT also suppose that the transverse shear strains γ_{13} and γ_{23} vanish.

Thus, equation (A-5) reduces to

$$
\begin{Bmatrix} D_1 \\ D_2 \\ D_3 \end{Bmatrix} = \begin{pmatrix} 0 & 0 & 0 \\ 0 & 0 & 0 \\ \overline{e}_{31} & \overline{e}_{31} & 0 \end{pmatrix} \begin{Bmatrix} \varepsilon_{11} \\ \varepsilon_{22} \\ \gamma_{12} \end{Bmatrix} + \begin{pmatrix} \Xi_{11} & 0 & 0 \\ 0 & \Xi_{11} & 0 \\ 0 & 0 & \overline{\Xi}_{33} \end{pmatrix} \begin{Bmatrix} E_1 \\ E_2 \\ E_3 \end{Bmatrix}
$$

(A-9)

(3) For Plane Stress Problems

For plane stress problems,

$$\sigma_{33} = 0 \tag{A-10}$$

$$\sigma_{13} = \sigma_{23} = 0 \tag{A-11}$$

are assumed. Thus, ε_{33} can be expressed as equation (A-3) and γ_{13} and γ_{23} can be expressed as follows:

$$\gamma_{12} = \frac{e_{15}}{C_{55}^E} E_1, \qquad \gamma_{13} = \frac{e_{15}}{C_{55}^E} E_2. \tag{A-12}$$

The reduced constitutive relations can be obtained by substituting equation (A-12) into equations (A-1) and (A-2) as follows:

$$
\begin{Bmatrix} \sigma_{11} \\ \sigma_{22} \\ \sigma_{12} \end{Bmatrix} =
\begin{pmatrix}
\overline{C}_{11}^E & \overline{C}_{12}^E & 0 \\
\overline{C}_{12}^E & \overline{C}_{11}^E & 0 \\
0 & 0 & \frac{1}{2}(\overline{C}_{11}^E - \overline{C}_{12}^E)
\end{pmatrix}
\begin{Bmatrix} \varepsilon_{11} \\ \varepsilon_{22} \\ \gamma_{12} \end{Bmatrix} -
\begin{pmatrix}
0 & 0 & \overline{e}_{31} \\
0 & 0 & \overline{e}_{31} \\
0 & 0 & 0
\end{pmatrix}
\begin{Bmatrix} E_1 \\ E_2 \\ E_3 \end{Bmatrix}, \tag{A-13}
$$

$$
\begin{Bmatrix} D_1 \\ D_2 \\ D_3 \end{Bmatrix} =
\begin{pmatrix}
0 & 0 & 0 \\
0 & 0 & 0 \\
\overline{e}_{31} & \overline{e}_{31} & 0
\end{pmatrix}
\begin{Bmatrix} \varepsilon_{11} \\ \varepsilon_{22} \\ \gamma_{12} \end{Bmatrix} +
\begin{pmatrix}
\Xi_{11}^{ps} & 0 & 0 \\
0 & \Xi_{11}^{ps} & 0 \\
0 & 0 & \overline{\overline{\Xi}}_{33}
\end{pmatrix}
\begin{Bmatrix} E_1 \\ E_2 \\ E_3 \end{Bmatrix}, \tag{A-14}
$$

where $\overline{C}_{11}^E$, $\overline{C}_{12}^E$, $\overline{e}_{31}$, and $\overline{\overline{\Xi}}_{33}$ are defined as in (A-6); Ξ_{11}^{ps} is given by

$$\Xi_{11}^{ps} = \Xi_{11} + \frac{e_{15}^2}{C_{55}^E}. \tag{A-15}$$

(4) For Plane Strain Problems

The plane strain assumptions, $\varepsilon_{33} = \gamma_{13} = \gamma_{23} = 0$, implies

102

$$\begin{Bmatrix} \sigma_{11} \\ \sigma_{22} \\ \sigma_{12} \end{Bmatrix} = \begin{pmatrix} C_{11}^E & C_{12}^E & 0 \\ C_{12}^E & C_{11}^E & 0 \\ 0 & 0 & \frac{1}{2}(C_{11}^E - C_{12}^E) \end{pmatrix} \begin{Bmatrix} \varepsilon_{11} \\ \varepsilon_{22} \\ \gamma_{12} \end{Bmatrix} - \begin{pmatrix} 0 & 0 & e_{31} \\ 0 & 0 & e_{31} \\ 0 & 0 & 0 \end{pmatrix} \begin{Bmatrix} E_1 \\ E_2 \\ E_3 \end{Bmatrix} \qquad \text{(A-16)}$$

$$\begin{Bmatrix} D_1 \\ D_2 \\ D_3 \end{Bmatrix} = \begin{pmatrix} 0 & 0 & 0 \\ 0 & 0 & 0 \\ e_{31} & e_{31} & 0 \end{pmatrix} \begin{Bmatrix} \varepsilon_{11} \\ \varepsilon_{22} \\ \gamma_{12} \end{Bmatrix} + \begin{pmatrix} \Xi_{11} & 0 & 0 \\ 0 & \Xi_{11} & 0 \\ 0 & 0 & \Xi_{33} \end{pmatrix} \begin{Bmatrix} E_1 \\ E_2 \\ E_3 \end{Bmatrix}. \qquad \text{(A-17)}$$

(5) For Beam Problems

The constitutive relations for beam problems can be derived on the basis of plane stress problems by assuming $\sigma_{22} = 0$, which implies

$$\varepsilon_{22} = \frac{\overline{e}_{31}}{\overline{C}_{11}^E} E_3 - \frac{\overline{C}_{12}^E}{\overline{C}_{11}^E} \varepsilon_{11}. \qquad \text{(A-18)}$$

Substituting equation (A-18) into equations (A-13) and (A-14) gives

$$\begin{Bmatrix} \sigma_{11} \\ \sigma_{12} \end{Bmatrix} = \begin{pmatrix} C_{11}^{Eb} & 0 \\ 0 & \frac{1}{2}(C_{11}^E - C_{12}^E) \end{pmatrix} \begin{Bmatrix} \varepsilon_{11} \\ \gamma_{12} \end{Bmatrix} - \begin{pmatrix} 0 & 0 & e_{31}^b \\ 0 & 0 & 0 \end{pmatrix} \begin{Bmatrix} E_1 \\ E_2 \\ E_3 \end{Bmatrix}, \qquad \text{(A-19)}$$

$$\begin{Bmatrix} D_1 \\ D_2 \\ D_3 \end{Bmatrix} = \begin{pmatrix} 0 & 0 \\ 0 & 0 \\ e_{31}^b & 0 \end{pmatrix} \begin{Bmatrix} \varepsilon_{11} \\ \gamma_{12} \end{Bmatrix} + \begin{pmatrix} \Xi_{11}^{ps} & 0 & 0 \\ 0 & \Xi_{11}^{ps} & 0 \\ 0 & 0 & \Xi_{33}^b \end{pmatrix} \begin{Bmatrix} E_1 \\ E_2 \\ E_3 \end{Bmatrix}, \qquad \text{(A-20)}$$

where Ξ_{11}^{ps} has been given by (A-15); C_{11}^{Eb}, e_{31}^b, and Ξ_{33}^b are given by

103

$$C_{11}^{Eb} = C_{11}^E + \frac{C_{11}^E(C_{13}^E)^2 - 2C_{12}^E(C_{13}^E)^2 + (C_{12}^E)^2 C_{33}^E}{(C_{13}^E)^2 - C_{11}^E C_{33}^E},$$

$$e_{31}^b = \frac{(C_{11}^E - C_{12}^E)(C_{33}^E e_{31} - C_{13}^E e_{33})}{C_{11}^E C_{33}^E - (C_{13}^E)^2}, \qquad (\text{A-21})$$

$$\Xi_{33}^b = \Xi_{33} + \frac{e_{33}^2}{C_{33}^E} + \frac{(C_{33}^E e_{31} - C_{13}^E e_{33})^2}{C_{33}^E[C_{11}^E C_{33}^E - (C_{13}^E)^2]}.$$

A.2 Poling Direction in Axis 2

If we denote

$$\overline{C}_{11}^E = C_{11}^E - \frac{(C_{12}^E)^2}{C_{11}^E}, \quad \overline{C}_{13}^E = C_{13}^E - \frac{C_{12}^E C_{13}^E}{C_{11}^E}, \quad \overline{C}_{33}^E = C_{33}^E - \frac{(C_{13}^E)^2}{C_{11}^E},$$

$$\overline{e}_{31} = e_{31} - \frac{C_{12}^E}{C_{11}^E} e_{31}, \quad \overline{e}_{33} = e_{33} - \frac{C_{13}^E}{C_{11}^E} e_{31}, \quad \overline{\overline{\Xi}}_{33} = \Xi_{33} + \frac{e_{31}^2}{C_{11}^E},$$

$$(\text{A-22})$$

$$\Xi_{11}^{ps} = \Xi_{11} + \frac{e_{15}^2}{C_{55}^E},$$

$$C_{11}^{Eb} = C_{11}^E + \frac{C_{11}^E(C_{13}^E)^2 - 2C_{12}^E(C_{13}^E)^2 + (C_{12}^E)^2 C_{33}^E}{(C_{13}^E)^2 - C_{11}^E C_{33}^E},$$

$$e_{31}^b = \frac{(C_{11}^E - C_{12}^E)(C_{33}^E e_{31} - C_{13}^E e_{33})}{C_{11}^E C_{33}^E - (C_{13}^E)^2},$$

$$\Xi_{33}^b = \Xi_{33} + \frac{e_{31}^2}{C_{11}^E} + \frac{(C_{13}^E e_{31} - C_{11}^E e_{33})^2}{C_{11}^E [C_{11}^E C_{33}^E - (C_{13}^E)^2]},$$

the constitutive relationships for IPT, CPT, plane stress problems, plane strain problems and beams can be expressed as follows:

(1) For the Mindlin's Plate Model (IPT)

$$\begin{Bmatrix} \sigma_{11} \\ \sigma_{22} \\ \sigma_{12} \\ \sigma_{13} \\ \sigma_{23} \end{Bmatrix} = \begin{pmatrix} \overline{C}_{11}^E & \overline{C}_{13}^E & 0 & 0 & 0 \\ \overline{C}_{13}^E & \overline{C}_{33}^E & 0 & 0 & 0 \\ 0 & 0 & C_{55}^E & 0 & 0 \\ 0 & 0 & 0 & \dfrac{\kappa^2}{2}(C_{11}^E - C_{12}^E) & 0 \\ 0 & 0 & 0 & 0 & \kappa^2 C_{55}^E \end{pmatrix} \begin{Bmatrix} \varepsilon_{11} \\ \varepsilon_{22} \\ \gamma_{12} \\ \gamma_{13} \\ \gamma_{23} \end{Bmatrix}$$

$$- \begin{pmatrix} 0 & \overline{e}_{31} & 0 \\ 0 & \overline{e}_{33} & 0 \\ e_{15} & 0 & 0 \\ 0 & 0 & 0 \\ 0 & 0 & e_{15} \end{pmatrix} \begin{Bmatrix} E_1 \\ E_2 \\ E_3 \end{Bmatrix}, \tag{A-23}$$

$$\begin{Bmatrix} D_1 \\ D_2 \\ D_3 \end{Bmatrix} = \begin{pmatrix} 0 & 0 & e_{15} & 0 & 0 \\ \overline{e}_{31} & \overline{e}_{33} & 0 & 0 & 0 \\ 0 & 0 & 0 & 0 & e_{15} \end{pmatrix} \begin{Bmatrix} \varepsilon_{11} \\ \varepsilon_{22} \\ \gamma_{12} \\ \gamma_{13} \\ \gamma_{23} \end{Bmatrix} + \begin{pmatrix} \Xi_{11} & 0 & 0 \\ 0 & \overline{\Xi}_{33} & 0 \\ 0 & 0 & \Xi_{11} \end{pmatrix} \begin{Bmatrix} E_1 \\ E_2 \\ E_3 \end{Bmatrix} \tag{A-24}$$

;

(2) For the Kirchhoff's Plate Model (CPT)

$$\begin{Bmatrix} \sigma_{11} \\ \sigma_{22} \\ \sigma_{12} \end{Bmatrix} = \begin{pmatrix} \overline{C}^E_{11} & \overline{C}^E_{13} & 0 \\ \overline{C}^E_{13} & \overline{C}^E_{33} & 0 \\ 0 & 0 & C^E_{55} \end{pmatrix} \begin{Bmatrix} \varepsilon_{11} \\ \varepsilon_{22} \\ \gamma_{12} \end{Bmatrix} - \begin{pmatrix} 0 & \overline{e}_{31} & 0 \\ 0 & \overline{e}_{33} & 0 \\ e_{15} & 0 & 0 \end{pmatrix} \begin{Bmatrix} E_1 \\ E_2 \\ E_3 \end{Bmatrix} \tag{A-25}$$

$$\begin{Bmatrix} D_1 \\ D_2 \\ D_3 \end{Bmatrix} = \begin{pmatrix} 0 & 0 & e_{15} \\ \overline{e}_{31} & \overline{e}_{33} & 0 \\ 0 & 0 & 0 \end{pmatrix} \begin{Bmatrix} \varepsilon_{11} \\ \varepsilon_{22} \\ \gamma_{12} \end{Bmatrix} + \begin{pmatrix} \Xi_{11} & 0 & 0 \\ 0 & \overline{\Xi}_{33} & 0 \\ 0 & 0 & \Xi_{11} \end{pmatrix} \begin{Bmatrix} E_1 \\ E_2 \\ E_3 \end{Bmatrix} \tag{A-26}$$

(3) For Plane Stress Problems

$$\begin{Bmatrix} \sigma_{11} \\ \sigma_{22} \\ \sigma_{12} \end{Bmatrix} = \begin{pmatrix} \overline{C}^E_{11} & \overline{C}^E_{13} & 0 \\ \overline{C}^E_{13} & \overline{C}^E_{33} & 0 \\ 0 & 0 & C^E_{55} \end{pmatrix} \begin{Bmatrix} \varepsilon_{11} \\ \varepsilon_{22} \\ \gamma_{12} \end{Bmatrix} - \begin{pmatrix} 0 & \overline{e}_{31} & 0 \\ 0 & \overline{e}_{33} & 0 \\ e_{15} & 0 & 0 \end{pmatrix} \begin{Bmatrix} E_1 \\ E_2 \\ E_3 \end{Bmatrix} \tag{A-27}$$

$$\begin{Bmatrix} D_1 \\ D_2 \\ D_3 \end{Bmatrix} = \begin{pmatrix} 0 & 0 & e_{15} \\ \overline{e}_{31} & \overline{e}_{33} & 0 \\ 0 & 0 & 0 \end{pmatrix} \begin{Bmatrix} \varepsilon_{11} \\ \varepsilon_{22} \\ \gamma_{12} \end{Bmatrix} + \begin{pmatrix} \Xi_{11} & 0 & 0 \\ 0 & \overline{\Xi}_{33} & 0 \\ 0 & 0 & \Xi^{ps}_{11} \end{pmatrix} \begin{Bmatrix} E_1 \\ E_2 \\ E_3 \end{Bmatrix} \tag{A-28}$$

(4) For Plane Strain Problems

$$\begin{Bmatrix} \sigma_{11} \\ \sigma_{22} \\ \sigma_{12} \end{Bmatrix} = \begin{pmatrix} C^E_{11} & C^E_{13} & 0 \\ C^E_{13} & C^E_{33} & 0 \\ 0 & 0 & C^E_{55} \end{pmatrix} \begin{Bmatrix} \varepsilon_{11} \\ \varepsilon_{22} \\ \gamma_{12} \end{Bmatrix} - \begin{pmatrix} 0 & e_{31} & 0 \\ 0 & e_{33} & 0 \\ e_{15} & 0 & 0 \end{pmatrix} \begin{Bmatrix} E_1 \\ E_2 \\ E_3 \end{Bmatrix} \tag{A-29}$$

$$\begin{Bmatrix} D_1 \\ D_2 \\ D_3 \end{Bmatrix} = \begin{pmatrix} 0 & 0 & e_{15} \\ e_{31} & e_{33} & 0 \\ 0 & 0 & 0 \end{pmatrix} \begin{Bmatrix} \varepsilon_{11} \\ \varepsilon_{22} \\ \gamma_{12} \end{Bmatrix} + \begin{pmatrix} \Xi_{11} & 0 & 0 \\ 0 & \Xi_{33} & 0 \\ 0 & 0 & \Xi_{11} \end{pmatrix} \begin{Bmatrix} E_1 \\ E_2 \\ E_3 \end{Bmatrix} \tag{A-30}$$

(5) For Beam Problems

$$\left\{\begin{matrix} \sigma_{11} \\ \sigma_{12} \end{matrix}\right\} = \begin{pmatrix} C_{11}^{Eb} & 0 \\ 0 & C_{55}^{E} \end{pmatrix} \left\{\begin{matrix} \varepsilon_{11} \\ \gamma_{12} \end{matrix}\right\} - \begin{pmatrix} 0 & e_{31}^{b} & 0 \\ e_{15} & 0 & 0 \end{pmatrix} \left\{\begin{matrix} E_1 \\ E_2 \\ E_3 \end{matrix}\right\} , \tag{A-31}$$

$$\left\{\begin{matrix} D_1 \\ D_2 \\ D_3 \end{matrix}\right\} = \begin{pmatrix} 0 & e_{15} \\ e_{31}^{b} & 0 \\ 0 & 0 \end{pmatrix} \left\{\begin{matrix} \varepsilon_{11} \\ \gamma_{12} \end{matrix}\right\} + \begin{pmatrix} \Xi_{11} & 0 & 0 \\ 0 & \Xi_{33}^{b} & 0 \\ 0 & 0 & \Xi_{11}^{ps} \end{pmatrix} \left\{\begin{matrix} E_1 \\ E_2 \\ E_3 \end{matrix}\right\} . \tag{A-32}$$

A.3 Poling Direction in Axis 1

If we denote

$$\overline{C}_{11}^{E} = C_{11}^{E} - \frac{(C_{12}^{E})^2}{C_{11}^{E}} , \quad \overline{C}_{13}^{E} = C_{13}^{E} - \frac{C_{12}^{E} C_{13}^{E}}{C_{11}^{E}} , \quad \overline{C}_{33}^{E} = C_{33}^{E} - \frac{(C_{13}^{E})^2}{C_{11}^{E}} ,$$

$$\overline{e}_{31} = e_{31} - \frac{C_{12}^{E}}{C_{11}^{E}} e_{31} , \quad \overline{e}_{33} = e_{33} - \frac{C_{13}^{E}}{C_{11}^{E}} e_{31} , \quad \overline{\Xi}_{33} = \Xi_{33} + \frac{e_{31}^2}{C_{11}^{E}} ,$$

$$\Xi_{11}^{ps} = \Xi_{11} + \frac{e_{15}^2}{C_{55}^{E}} , \tag{A-33}$$

$$C_{33}^{Eb} = C_{33}^{E} - \frac{2(C_{13}^{E})^2}{C_{11}^{E} + C_{12}^{E}} ,$$

$$e_{33}^{b} = e_{33} - \frac{2C_{13}^{E}}{C_{11}^{E} + C_{12}^{E}} e_{31} ,$$

$$\Xi_{33}^b = \Xi_{33} + \frac{2e_{31}^2}{C_{11}^E + C_{12}^E},$$

the constitutive relationships for IPT, CPT, plane stress problems, plane strain problems and beams can be expressed as follows:

(2) For the Mindlin's Plate Model (IPT)

$$
\begin{Bmatrix} \sigma_{11} \\ \sigma_{22} \\ \sigma_{12} \\ \sigma_{13} \\ \sigma_{23} \end{Bmatrix} =
\begin{pmatrix}
\overline{C}_{33}^E & \overline{C}_{13}^E & 0 & 0 & 0 \\
\overline{C}_{13}^E & \overline{C}_{11}^E & 0 & 0 & 0 \\
0 & 0 & C_{55}^E & 0 & 0 \\
0 & 0 & 0 & \kappa^2 C_{55}^E & 0 \\
0 & 0 & 0 & 0 & \dfrac{\kappa^2}{2}(C_{11}^E - C_{12}^E)
\end{pmatrix}
\begin{Bmatrix} \varepsilon_{11} \\ \varepsilon_{22} \\ \gamma_{12} \\ \gamma_{13} \\ \gamma_{23} \end{Bmatrix}
$$
$$
-\begin{pmatrix}
\overline{e}_{33} & 0 & 0 \\
\overline{e}_{31} & 0 & 0 \\
0 & e_{15} & 0 \\
0 & 0 & e_{15} \\
0 & 0 & 0
\end{pmatrix}
\begin{Bmatrix} E_1 \\ E_2 \\ E_3 \end{Bmatrix},
$$

(A-34)

$$
\begin{Bmatrix} D_1 \\ D_2 \\ D_3 \end{Bmatrix} =
\begin{pmatrix}
\overline{e}_{33} & \overline{e}_{31} & 0 & 0 & 0 \\
0 & 0 & e_{15} & 0 & 0 \\
0 & 0 & 0 & e_{15} & 0
\end{pmatrix}
\begin{Bmatrix} \varepsilon_{11} \\ \varepsilon_{22} \\ \gamma_{12} \\ \gamma_{13} \\ \gamma_{23} \end{Bmatrix}
+
\begin{pmatrix}
\overline{\Xi}_{33} & 0 & 0 \\
0 & \Xi_{11} & 0 \\
0 & 0 & \Xi_{11}
\end{pmatrix}
\begin{Bmatrix} E_1 \\ E_2 \\ E_3 \end{Bmatrix}
$$

(A-35)

;

(2) For the Kirchhoff's Plate Model (CPT)

$$
\begin{Bmatrix} \sigma_{11} \\ \sigma_{22} \\ \sigma_{12} \end{Bmatrix} =
\begin{pmatrix}
\overline{C}_{33}^E & \overline{C}_{13}^E & 0 \\
\overline{C}_{13}^E & \overline{C}_{11}^E & 0 \\
0 & 0 & C_{55}^E
\end{pmatrix}
\begin{Bmatrix} \varepsilon_{11} \\ \varepsilon_{22} \\ \gamma_{12} \end{Bmatrix}
-
\begin{pmatrix}
\overline{e}_{33} & 0 & 0 \\
\overline{e}_{31} & 0 & 0 \\
0 & e_{15} & 0
\end{pmatrix}
\begin{Bmatrix} E_1 \\ E_2 \\ E_3 \end{Bmatrix},
$$

(A-36)

$$\begin{Bmatrix} D_1 \\ D_2 \\ D_3 \end{Bmatrix} = \begin{pmatrix} \overline{e}_{33} & \overline{e}_{31} & 0 \\ 0 & 0 & e_{15} \\ 0 & 0 & 0 \end{pmatrix} \begin{Bmatrix} \varepsilon_{11} \\ \varepsilon_{22} \\ \gamma_{12} \end{Bmatrix} + \begin{pmatrix} \overline{\Xi}_{33} & 0 & 0 \\ 0 & \Xi_{11} & 0 \\ 0 & 0 & \Xi_{11} \end{pmatrix} \begin{Bmatrix} E_1 \\ E_2 \\ E_3 \end{Bmatrix} ; \tag{A-37}$$

(3) For Plane Stress Problems

$$\begin{Bmatrix} \sigma_{11} \\ \sigma_{22} \\ \sigma_{12} \end{Bmatrix} = \begin{pmatrix} \overline{C}_{33}^E & \overline{C}_{13}^E & 0 \\ \overline{C}_{13}^E & \overline{C}_{11}^E & 0 \\ 0 & 0 & C_{55}^E \end{pmatrix} \begin{Bmatrix} \varepsilon_{11} \\ \varepsilon_{22} \\ \gamma_{12} \end{Bmatrix} - \begin{pmatrix} \overline{e}_{33} & 0 & 0 \\ \overline{e}_{31} & 0 & 0 \\ 0 & e_{15} & 0 \end{pmatrix} \begin{Bmatrix} E_1 \\ E_2 \\ E_3 \end{Bmatrix} , \tag{A-38}$$

$$\begin{Bmatrix} D_1 \\ D_2 \\ D_3 \end{Bmatrix} = \begin{pmatrix} \overline{e}_{33} & \overline{e}_{31} & 0 \\ 0 & 0 & e_{15} \\ 0 & 0 & 0 \end{pmatrix} \begin{Bmatrix} \varepsilon_{11} \\ \varepsilon_{22} \\ \gamma_{12} \end{Bmatrix} + \begin{pmatrix} \overline{\Xi}_{33} & 0 & 0 \\ 0 & \Xi_{11} & 0 \\ 0 & 0 & \Xi_{11}^{ps} \end{pmatrix} \begin{Bmatrix} E_1 \\ E_2 \\ E_3 \end{Bmatrix} ; \tag{A-39}$$

(4) For Plane Strain Problems

$$\begin{Bmatrix} \sigma_{11} \\ \sigma_{22} \\ \sigma_{12} \end{Bmatrix} = \begin{pmatrix} C_{33}^E & C_{13}^E & 0 \\ C_{13}^E & C_{11}^E & 0 \\ 0 & 0 & C_{55}^E \end{pmatrix} \begin{Bmatrix} \varepsilon_{11} \\ \varepsilon_{22} \\ \gamma_{12} \end{Bmatrix} - \begin{pmatrix} e_{33} & 0 & 0 \\ e_{31} & 0 & 0 \\ 0 & e_{15} & 0 \end{pmatrix} \begin{Bmatrix} E_1 \\ E_2 \\ E_3 \end{Bmatrix} , \tag{A-40}$$

$$\begin{Bmatrix} D_1 \\ D_2 \\ D_3 \end{Bmatrix} = \begin{pmatrix} e_{33} & e_{31} & 0 \\ 0 & 0 & e_{15} \\ 0 & 0 & 0 \end{pmatrix} \begin{Bmatrix} \varepsilon_{11} \\ \varepsilon_{22} \\ \gamma_{12} \end{Bmatrix} + \begin{pmatrix} \Xi_{33} & 0 & 0 \\ 0 & \Xi_{11} & 0 \\ 0 & 0 & \Xi_{11} \end{pmatrix} \begin{Bmatrix} E_1 \\ E_2 \\ E_3 \end{Bmatrix} ; \tag{A-41}$$

(6) For Beam Problems

$$\begin{Bmatrix} \sigma_{11} \\ \sigma_{12} \end{Bmatrix} = \begin{pmatrix} C_{33}^{Eb} & 0 \\ 0 & C_{55}^E \end{pmatrix} \begin{Bmatrix} \varepsilon_{11} \\ \gamma_{12} \end{Bmatrix} - \begin{pmatrix} e_{33}^b & 0 & 0 \\ 0 & e_{15} & 0 \end{pmatrix} \begin{Bmatrix} E_1 \\ E_2 \\ E_3 \end{Bmatrix} , \tag{A-42}$$

$$\begin{Bmatrix} D_1 \\ D_2 \\ D_3 \end{Bmatrix} = \begin{pmatrix} e_{33}^b & 0 \\ 0 & e_{15} \\ 0 & 0 \end{pmatrix} \begin{Bmatrix} \varepsilon_{11} \\ \gamma_{12} \end{Bmatrix} + \begin{pmatrix} \Xi_{33}^b & 0 & 0 \\ 0 & \Xi_{11} & 0 \\ 0 & 0 & \Xi_{11}^{ps} \end{pmatrix} \begin{Bmatrix} E_1 \\ E_2 \\ E_3 \end{Bmatrix} \qquad \text{(A-43)}$$

110

LIST OF REFERENCES

1) Allik, H. and T.J.R. Hughes. 1970. Finite element method for piezoelectric vibration. Internationalcal Methods in Engineering 2:151-157.

2) Bailey, T. and J.E. Hubbard. 1985. Distributed piezoelectric-polymer active vibration control of a cantilever beam. Journal of Guidance 8:605-611.

3) Batra, R.C. and X. Q. Liang.1997. The vibration of a rectangular laminated elastic plate with embedded piezoelectric sensors and actuators. Computers and Structures 63:203-216.

4) Baz, A. and S. Poh. 1988. Performance of an active control system with piezoelectric actuators. Journal of Sound and Vibration 126:327-343.

5) Bhattacharya, P., H. Suhail, and P.K. Sinha. 1998. Finite element free vibration analysis of smart laminated composite beams and plates. Journal of Intelligent Material Systems and Structures 9:20-28.

6) Chandrashekhara, K. and A.N. Agarwal. 1993. Active vibration control of laminated composite plates using piezoelectric devices: a finite element approach. Journal of Intelligent Material Systemsand Structures 4:496-508.

7) Chandrashekhara, K. and R. Tenneti. 1995. Thermally induced vibration suppression of laminated plates with piezoelectric sensors and actuators. Smart Materials and Structures 4:281-290.

8) Chandrashekhara, K. and S. Varadarajan. 1997. Adaptive shape control of composite beams with piezoelectric actuators. Journal of Intelligent Material Systems and Structures 8:112-124.

9) Chattopadhyay, A., H. Gu, and D. Dragomir-Daescu. 1999. Dynamics of delaminated composite plates with piezoelectric actuators. AIAA Journal 37:248-254.

10) Chattopadhyay, A. and C. Seeley. 1997. A higher order theory for modeling composite laminates with induced strain actuators. Composites Part B 28B:243-252.

11) Clark, R.L., C.R. Fuller, and A. Wicks. 1991. Characterization of multiple piezoelectric actuators for structural excitation. Journal of the Acoustical Society of America 90:346-357.

12) Cook, R.D., D.S. Malkus, and M.E. Plesha. 1989. Concepts and Applications of Finite Element Analysis, Third Edition. New York: John Wiley & Sons.

13) Crawley, E.F. 1994. Intelligent structures for aerospace: a technology overview and assessment. AIAA Journal 32:1689-1699.

14) Crawley, E.F. and E.H. Anderson. 1990. Detailed models of piezoceramic actuation of beams. Journal of Intelligent Material Systems and Structures 1:4-25.

15) Crawley, E.F. and J. de Luis. 1987. Use of piezoelectric actuators as elements of intelligent structures. AIAA Journal 25:1373-1385.

16) Crawley, E.F. and K. B. Lazarus. 1991. Induced strain actuation of isotropic and anisotropic plates. AIAA Journal 29:944-951.

17) Daniel, I.M. and O. Ishai. 1994. Engineering Mechanics of Composite Materials. New York: Oxford University Press.

18) Dimitriadis, E.K., C.R. Fuller and C.A. Rogers. 1991. Piezoelectric actuators for distributed vibration excitation of thin plates. Journal of Vibration and Acoustics 113:100-107.

19) Donthireddy, P. and K. Chandrashekhara. 1996. Modeling and shape control of composite beams with embedded piezoelectric actuators. Composite Structures 35:237-244.

20) Friswell, M.I., D.J. Inman, and R.W. Rietz. 1997. Active damping of thermally induced vibrations. Journal of Intelligent Material Systems and Structures 8:678-685.

21) Fung, Y.C. 1965. Foundations of solid mechanics. Englewood Cliffs, New Jersey: Prentice-Hall, Inc.

22) Ha, S.K., C. Keilers and F-K. Chang. 1992. Finite element analysis of composite structures containing distributed piezoceramic sensors and actuators. AIAA Journal 30:772-780.

23) Heyliger, P.R., K.C. Pei, and D.A. Saravanos. 1996. Layerwise mechanics and finite element model for laminated piezoelectric shells. AIAA Journal 34:2353-2360.

24) Heyliger, P.R., G. Ramirez, and D. Saravanos. 1994. Coupled discrete-layer finite elements for laminated piezoelectric plates. Communications in Numerical Methods in Engineering 10:971-981.

25) Heyliger, P.R. and D.A. Saravanos. 1995. Exact free-vibration analysis of laminated plates with embedded piezoelectric layers. Journal of the Acoustical Society of America 98:1-11.

26) Hong, C.-H. and I. Chopra. 1999. Modeling and validation of induced strain actuation of composite coupled plates. AIAA Journal 37:372-377.

27) Hughes, T.J.R. 1987. The Finite Element Method, Third Edition. Englewood Cliffs, New Jersey: Prentice-Hall, Inc.

28) Hwang, W.-S. and H.C. Park. 1993. Finite element modeling of piezoelectric sensors and actuators. AIAA Journal 31:930-937.

29) Im, S. and S.N. Atluri. 1989. Effects of a piezo-actuator on a finitely deformed beam subjected to general loading. AIAA Journal 27:1801-1807.

30) Jonnalagadda, K.D., G.E. Blandford, and T.R. Tauchert. 1994. Piezothermoelastic composite plate analysis using first-order shear deformation theory. Computers and Structures 51:79-89.

31) Kim, J., V.V. Varadan, and V.K. Varadan.1997. Finite element modelling of structures including piezoelectric active devices. International Journal for Numerical Methods in Engineering 40:817-832.

32) Kim, J., V.V. Varadan, V.K. Varadan and X.-Q. Bao. 1996. Finite-element modeling of a smart cantilever plate and comparison with experiments. Smart Materials and Structures 5:165-170.

33) Koconis, D.B., L.P. Kollar, and G.S. Springer. 1994a. Shape control of composite plates and shells with embedded actuators. I. Voltages specified. Journal of Composite Materials 28:415-458.

34) Koconis, D.B., L.P. Kollar, and G.S. Springer. 1994b. Shape control of composite plates and shells with embedded actuators. II. Desired shape specified. Journal of Composite Materials 28:459-483.

35) Lam, K.Y., X.Q. Peg, G.R. Liu, and J.N. Reddy. 1997. A finite-element model for piezoelectric composite laminates. Smart Materials and Structures 6:583-591.

36) Lammering, R. 1991. The application of a finite shell element for composites containing piezo-electric polymers in vibration control. Computers and Structures 41:1101-1109.

114

37) Lee, C.-K. 1990. Theory of laminated piezoelectric plates for the design of distributed sensors/actuators. Part I: Governing equations and reciprocal relationships. Journal of the Acoustical Society of America 87:1144-1158.

38) Lee, C.-K., W.-W. Chiang, and T.C. O'Sullivan. 1991. Piezoelectric modal sensor/actuator pairs for critical active damping vibration control. Journal of the Acoustical Society of America 90:374-384.

39) Lee, C.-K. and F.C. Moon.1989. Laminated piezopolymer plates for torsion and bending sensors and actuators. Journal of the Acoustical Society of America 85:2432-2439.

40) Lee, H.-J. And D.A. Saravanos. 1996. Coupled layerwise analysis of thermopiezoelectric composite beams. AIAA Journal 34:1231-1237.

41) Lee, H.-J. And D.A. Saravanos. 1997. Generalized finite element formulation for smart multilayered thermal piezoelectric composite plates. International Journal of Solids and Structures 34:3355-3371.

42) Lee, H.-J. And D.A. Saravanos. 1998. The effect of temperature dependent material properties on the response of piezoelectric composite materials. Journal of Intelligent Material Systems and Structures 9:503-508.

43) Lee, H.-J. And D.A. Saravanos. 2000. A mixed multi-field finite element formulation for thermopiezoelectric composite shells. International Journal of Solids and Structures 37:4949-4967.

44) Lerch, R. 1990. Simulation of piezoelectric devices by two- and three-dimensional finite elements. IEEE Transactions on Ultrasonics, Ferroelectrics, and Frequency Control 37:233-247.

45) Librescu, L., L. Meirovitch and S.S. Na. 1997. Control of cantilever vibration via structural tailoring and adaptive materials. AIAA Journal 35:1309-1315.

46) Lin, C.-C., C.-Y. Hsu and H.-N. Huang. 1996. Finite element analysis on deflection control of plates with piezoelectric actuators. Composite Structures 35:423-433.

47) Liu, G.R., X.Q. Peng and K.Y. Lam. 1999. Vibration control simulation of laminated composite plates with integrated piezoelectrics. Journal of Sound and Vibration 220:827-846.

48) Loewy, R.G. 1997. Recent developments in smart structures with aeronautical applications. SmartMaterials and Structures 6:R11-R42.

49) Mason, W.P. 1950. Piezoelectric crystals and their application to ultrasonics. New York: D. Van Nostrand Company, Inc. Mindlin, R.D. 1974. Equations of high frequency vibrations of thermopiezoelectric crystal plates. International Journal of Solids and Structures 10:625-637.

50) Mitchell, J.A. and J.N. Reddy. 1995a. A refined hybrid plate theory for composite laminates with piezoelectric laminae. International Journal of Solids and Structures 32:2345-2367.

51) Mitchell, J.A. and J.N. Reddy. 1995b. A study of embedded piezoelectric layers in composite cylinders. Journal of Applied Mechanics 62:166-173.

52) Naillon, M., R.H. Coursant, and F. Besnier. 1983. Analysis of piezoelectric structures by a finite element method. ACTA Electronica 25:341-362.

53) Nye, J.F. 1964. Physical properties of crystals. Oxford: The Clarendon Press. Oguamanam, D.C.D., S.F.M. Almeida, and J.S. Hansen. 1998. Stress stiffening effects in

laminated beams with piezoelectric actuators. Journal of Intelligent Material Systems and Structures 9:137-145.

54) Pai, P.F., A.H. Nayfeh, K. Oh and D.T. Mook. 1993. A refined nonlinear model of composite plates with integrated piezoelectric actuators and sensors. International Journal of Solids and Structures 30:1603-1630.

55) Park, C. and I. Chopra. 1996. Modeling piezoceramic actuation of beams in torsion. AIAA Journal 34:2582-2589.

56) Parton, V.Z. and B.A. Kudryavtsev.1988. Electromagnetoelasticity. New York: Gordon and Breach Science Publishers. Peng, X.Q., K.Y. Lam, and G.R. Liu. 1998. Active vibration control of composite beams with piezoelectrics: a finite element model with third order theory. Journal of Sound and Vibration 209:635-650.

57) Pletner, B. and H. Abramovich. 1997. Consistent methodology for the modeling of piezolaminated shells. AIAA Journal 35:1316-1326.

58) Rao, S.S. and M. Sunar. 1993. Analysis of distributed thermopiezoelectric sensors and actuators in advanced intelligent structures. AIAA Journal 31:1280-1286.

59) Ray, M.C., R. Bhattacharyya, and B. Samanta. 1994. Static analysis of an intelligent structure by the finite element method. Computers and Structures 52:617-631.

60) Reddy, J.N. 1993. An evaluation of equivalent-single-layer and layerwise theories of composite laminates. Composite Structures 25:21-35.

61) Robbins, D.H. and J.N. Reddy. 1991. Analysis of piezoelectrically actuated beams using a layer-wise displacement theory. Computers and Structures 41:265-279.

62) Samanta, B., M.C. Ray and R. Bhattacharyya. 1996. Finite element model for active control of intelligent structures. AIAA Journal 34:1885-1893.

63) Saravanos, D.A. 1997. Mixed laminate theory and finite element for smart piezoelectric composite shell structures. AIAA Journal 35:1327-1333.

64) Saravanos, D.A.and P.R. Heyliger. 1995. Coupled layerwise analysis of composite beams with embedded piezoelectric sensors and actuators. Journal of Intelligent Material Systems and Structures 6:350-363.

65) Shen, M.-H. 1995. A new modeling technique for piezoelectrically actuated beams. Computers and Structures 57:361-366.

66) Shen, Y.-C. and C.-I Weng. 1995. Deformation control of laminated composite plates containing piezoelectric layers under thermal loading. Journal of Thermal Stresses 18:449-464.

67) Shieh, R.C. 1994. Governing equations and finite element models for multiaxial piezoelectric beam sensors/actuators. AIAA Journal 32:1250-1258.

68) Simitses, G. J, S. Sallam and W. L. Yin. 1985. Effect of delamination of axially loaded homogeneous laminated plates. AIAA Journal 23:1437-1444.

69) Soedel, W. 1993. Deep shell equations, vibrations of shells and plates. New York: Marcel Dekker, Inc. Stam, M. and G. Carman. 1996. Electrothermoelastic behavior of piezoelectric coupled cylinders. AIAA Journal 34:1612-1618.

70) Suleman, A. and V.B. Venkayya. 1995. A simple finite element formulation for a laminated composite plate with piezoelectric layers. Journal of Intelligent Material Systems and Structures 6:776-782.

71) Sunar, M. and S.S. Rao. 1997. Thermopiezoelectric control design and actuator placement. AIAA Journal 35:534-539.

72) Sung, C.K., T.F. Chen and S.G. Chen. 1996. Piezoelectric modal sensor/actuator design for monitoring/generating flexural and torsional vibrations of cylindrical shells. Journal of Vibration and Acoustics 118:48-55.

73) Tang, Y.Y. and K. Xu. 1995. Dynamic analysis of a piezothermoelastic laminate plate. Journal of Thermal Stresses 18:87-104.

74) Tauchert, T.R. 1992. Piezothermoelastic behavior of a laminated plate. Journal of Thermal Stresses 15:25-37.

75) Tiersten, H.F. 1969. Linear piezoelectric plate vibrations. New York: Plenum Press.Tong, D., R. Williams II, and S.K. Agrawal. 1998. Optimal shape control of composite thin plates with piezoelectric actuators. Journal of Intelligent Material Systems and Structures 9:458-467.

76) Tzou, H.S. and Y. Bao. 1995. A theory on anisotropic piezothermoelastic shell laminates with sensors/actuator applications. Journal of Sound and Vibration 184:453-473.

77) Tzou, H.S. and M. Gadre. 1989. Theoretical analysis of a multi-layered thin shell coupled with piezoelectric shell actuators for distributed vibration controls. Journal of Sound and Vibration 132:433-450.

78) Tzou, H.S. and R.V. Howard. 1994. A piezothermoelastic thin shell theory applied to active structures. Journal of Vibration and Acoustics 116:295-302.

79) Tzou, H.S. and C.I. Tseng. 1990. Distributed piezoelectric sensor/actuator design for dynamic measurement/control of distributed parameter systems: a piezoelectric finite element approach. Journal of Sound and Vibration 138:17-34.

80) Tzou, H.S. and R. Ye. 1994. Piezothermoelasticity and precision control of piezoelectric systems:theory and finite element analysis. Journal of Vibration and Acoustics 116:489-495.

81) Wang, Q and S T Quek. 2004. Repair of delaminated beams via piezoelectric patches. Smart Materials and Structures 13:1222-1229.

82) Wang, Q. 2004. On the jump of buckling capacity of beams via piezoelectric layers. Advances in Structural Engineering 7:163-170.

83) Wang, Q and C. M. Wang. 2000. Optimal placement and size of piezoelectric patches on beams from controllability perspective. Smart Materials and Structures 9:558-567.

84) Wang, Q, S. T. Quek and K. M. Liew. 2002. On the repair of a cracked beam with a piezoelectric patch. Smart Materials and Structures 11:404-410.